DESIGN AND PROTOTYPING OF AN ELECTROMAGNETIC MEMS ENERGY HARVESTER FOR LOW FREQUENCY VIBRATIONS

A THESIS SUBMITTED TO
THE GRADUATE SCHOOL OF NATURAL AND APPLIED SCIENCES
OF
MIDDLE EAST TECHNICAL UNIVERSITY

BY

SEROL TÜRKYILMAZ

IN PARTIAL FULFILLMENT OF THE REQUIREMENTS
FOR
THE DEGREE OF MASTER OF SCIENCE
IN
ELECTRICAL AND ELECTRONICS ENGINEERING

SEPTEMBER 2011

Approval of the thesis:

DESIGN AND PROTOTYPING OF AN ELECTROMAGNETIC MEMS ENERGY HARVESTER FOR LOW FREQUENCY VIBRATIONS

submitted by **SEROL TÜRKYILMAZ** in partial fulfillment of the requirements for the degree of **Master of Science in Electrical and Electronics Engineering, Middle East Technical University** by,

Prof. Dr. Canan Özgen _____
Dean, Graduate School of **Natural and Applied Sciences**

Prof. Dr. İsmet Erkmen _____
Head of Department, **Electrical and Electronics Eng. Dept.**

Assoc. Prof. Dr. Haluk Külah _____
Supervisor, **Electrical and Electronics Eng. Dept., METU**

Examining Committee Members

Prof. Dr. Tayfun Akın _____
Electrical and Electronics Eng. Dept., METU

Assoc. Prof. Dr. Haluk Külah _____
Electrical and Electronics Eng. Dept., METU

Assist. Prof. Dr. Ali Muhtaroğlu _____
Electrical and Electronics Eng. Dept., METU-NCC

Assist. Prof. Dr. Barış Bayram _____
Electrical and Electronics Eng. Dept., METU

Dr. Özge Zorlu _____
METU MEMS Research & Application Center, METU

Date: 13.09.2011

I hereby declare that all information in this document has been obtained and presented in accordance with academic rules and ethical conduct. I also declare that, as required by these rules and conduct, I have fully cited and referenced all referenced material and results that are not original to this work.

Name, Surname: Serol Türkyılmaz

Signature:

ABSTRACT

DESIGN AND PROTOTYPING OF AN ELECTROMAGNETIC MEMS ENERGY HARVESTER FOR LOW FREQUENCY VIBRATIONS

Türkyılmaz, Serol

M. Sc., Department of Electrical and Electronics Engineering

Supervisor: Assoc. Prof. Dr. Haluk Külah

September 2011, 83 pages

This thesis study presents the design, simulation, and fabrication of a low frequency electromagnetic micro power generator. This power generator can effectively harvest energy from low frequency external vibrations (1-100 Hz). The main objective of the study is to increase the efficiency of the previously proposed structure in METU-MEMS Center, which uses the frequency up-conversion technique to harvest energy from low frequency vibration.

The proposed structure has been demonstrated by constructing several macro scale prototypes. In one of the constructed prototypes, the diaphragms are connected to a fixed frame via metal springs. The upper diaphragm having lower resonance frequency carries a magnet, and the lower diaphragm carries a hand wound coil and a magnetic piece for converting 6 Hz external vibrations up to 85 Hz, resulting a maximum voltage and power levels of 11.1 mV and 5.1 μW, respectively.

In an improved prototype, the metal springs are replaced with rubber ones, providing higher energy conversion efficiency and flexibility to tune the resonance frequency of both diaphragms to desired values. This prototype provides 104 μW maximum power and 37.7 mV maximum voltage in response to vibration levels of 30 Hz.

The proposed structure is also suitable to be realized by using microfabrication techniques. Hence, the structure to be microfabricated is studied and optimized for this purpose. When scaled to microelectromechanical dimensions, the expected maximum power and voltage from the 10 x 8.5 x 2.5 mm^3 generator is 119 nW and 15.2 mV, respectively. A microfabrication process has also been designed for the proposed generator structure. According to this process, the structure consists of a stack of two pieces, each carrying different diaphragms. The diaphragms are made of parylene, and the coil and the magnetic piece are electroplated copper and nickel, respectively.

As a result of this study, a new topology is proposed for harvesting energy at low frequency vibrations by the frequency up-conversion technique, and an efficiency improvement is expected with more than two orders of magnitude (119 nW output for the same size) compared to the study realized in our laboratory in converting low frequency (70-150 Hz) environmental vibrations to electrical energy.

Keywords: Micro power generator, Energy harvesting, Frequency up-conversion, Microelectromechanical systems (MEMS).

ÖZ

DÜŞÜK FREKANSLI TİTREŞİMLER İÇİN MEMS TABANLI
ELEKTROMANYETİK ENERJİ ÜRETECİ TASARIMI VE PROTOTİPLEMESİ

Türkyılmaz, Serol
Yüksek Lisans, Elektrik ve Elektronik Mühendisliği Bölümü
Tez Yöneticisi: Doç. Dr. Haluk Külah

Eylül 2011, 83 pages

Bu tez çalısmasında, düşük frekanslı bir elektromanyetik mikro enerji üretecinin tasarım, simülasyon ve mikro üretim süreçleri sunulmuştur. Bu üreteç ortamda zaten varolan düşük frekanslı çevresel titreşimleri (1-100 Hz) elektriksel enerjiye çevirebilmektedir. Bu çalışmanın amacı, METU-MEMS Araştırma Merkezi'nde geliştirilmiş olan düşük frekanslı titreşimlerden frekans yükseltme tekniği ile enerji elde edebilen yapının geliştirilmesi ve daha verimli çalışmasını sağlamaktır.

Önerilen tasarımın çalışması makro prototipler ile doğrulanmıştır. Metal yayların kullanıldığı bir prototipte, düşük frekanslı diyafram bir mıknatıs taşırken, yüksek frekanslı diyaframın üzerinde tel sarımları ve manyetik malzeme bulunmaktadır. Bu manyetik malzemenin mıknatıs tarafından yakalanıp bırakılması sonucu 6 Hz'lik çevresel titreşimler 85 Hz'lik titreşimlere yükseltilmektedir ve bunun sonucunda 11.1 mV gerilim ve 5.1 μW güç elde edilmektedir.

Geliştirilen başka bir prototipte daha yüksek güç değerlerine ulaşmak ve ayarlanabilir geniş bir frekans aralığında çalışabilmek için metal yayların yerini lastik yaylar almıştır. Bu prototip ile 30 Hz'lik titreşimlerde 37.7 mV gerilim ve 104 μW güç değerlerine ulaşılmıştır.

Önerilen yapı ayrıca mikro boyutta üretim için de uygun nitelikleri taşımaktadır. Tasarımın mikro boyutlarda üretilmesiyle, 10 x 8.5 x 2.5 mm^3 boyutlarındaki yapıdan 15.2 mV gerilim ve 119 nW güç seviyelerine ulaşılması beklenmektedir. Önerilen yapı için bir mikroüretim süreci önerilmiştir. Bu sürece göre enerji üreteci farklı diyaframların bulunduğu iki parça içermektedir ve bu iki parçanın birbirine yapıştırılması ile üretim sonlanmaktadır. Diyaframların üretiminde parylene malzemesi kullanılırken, tel sarımları ve manyetik malzeme bakır ve nikel kaplama teknikleri ile oluşturulmaktadır.

Bu çalışma sonucunda, düşük frekanslı titreşimlerden enerji elde etmek için frekans yükseltme metodu ile yeni bir tasarım önerilmiştir ve önceki çalışmaya göre 10 kattan fazla (119 nW) güç değerine ulaşılması beklenmektedir.

Anahtar kelimeler: Mikro güç üreteci, Enerji toplama, Frekans çevirimi, Mikroelektromekanik sistemler (MEMS).

To the One

and

To Serpil Türkyılmaz and Erol Türkyılmaz

ACKNOWLEDGMENTS

I would like to thank to my supervisor Assoc. Prof. Dr. Haluk Külah for his support and valuable comments for this thesis study. I am indebted to my supervisor for letting me pursue an M.Sc. study in PowerMEMS research group. I am also grateful to Assist. Prof. Dr. Ali Muhtaroğlu for his guidance throughout this study.

My sincere gratitude is for the METU-MEMS staff for the help and support during micro fabrication steps. I would like to thank to especially Orhan Akar and Dr. Özge Zorlu for the support during the micro fabrication steps. I would also like to thank to all my friends at the METU-MEMS group for their valuable discussions.

Finally, I would like to thank to my parents Serpil and Erol Türkyılmaz who have always supported me during this study. Without their support and patience, pursuing this study would only be a dream for me.

This work was supported by Intel Inc. under MER project (Middle East Energy Efficient Research project) and by TUBITAK under grant number 109E220.

TABLE OF CONTENTS

LIST OF TABLES

LIST OF FIGURES

CHAPTER 1

INTRODUCTION

Recent developments in microelectronics and MEMS (Micro-electromechanical systems) technology go through challenging improvements especially in portable low power and low cost electronic systems which includes sensors, actuators and micro switches. These systems have become an important part of our daily life by their low cost, small architecture, and enormous functionality. Some of the applications of these systems are; wireless sensor networks, structural health monitoring and military applications for powering devices on soldiers. As the size of these systems get smaller a compatibility problem with common energy sources arouses. Today, the most common energy sources for those kinds of systems are batteries. However, there is a bottleneck for delivering power to these systems with batteries because of their large dimensions. Also, the performance and energy densities of the batteries have not improved as fast as those of other microelectronic equipment in recent years [1]. Therefore, batteries have become disadvantageous for powering these systems both in terms of dimensional limits and in terms of performance parameters. Accordingly, there has been a trend to use already available energy sources as an alternative to batteries for powering these devices. Commonly available ambient energy sources are heat, light and vibration [2, 3]. Among these sources, vibration is particularly important due to its abundance, and therefore is in the main scope of this study. The following sections first summarize the various energy sources, and then provide the outline and scope of this thesis, which is the efficiency improvement of power generation at low frequency environmental vibrations.

1.1 Batteries as an Energy Source

Batteries are the most common energy sources for supplying power to electronic equipment used today. Unfortunately, apart from the invention of the battery, power and energy densities has not improved as fast as the improvement in microelectronics industry. Also, size of the batteries has not scaled down enough to be integrated with microsystems. Although size of the batteries have scaled down somehow in years, most of the batteries are still not compatible for integration into microelectronic or MEMS devices for an operation lifetime of few to tens of years. Therefore, alternative energy sources are required especially for small and micro autonomous systems.

Table 1.1. Comparison of energy harvesting sources together with batteries [6].

Energy Source	**Transduction Mechanism**	**Power Density ($\mu W/cm^3$) 1-year lifetime**	**Power Density ($\mu W/cm^3$) 10-year lifetime**
Solar	Photovoltaic	15,000 $_{sunny}$ 150 $_{cloudy}$	15,000 $_{sunny}$ 150 $_{cloudy}$
Vibration	**Piezoelectric Electrostatic Electromagnetic**	**4-800**	**4-800**
Temperature Gradient	Thermoelectric	60 @ 5ºC gradient	60 @ 5ºC gradient
Radio Frequency @ 2.4 GHz [35]	Electromagnetic Induction	400 @ 1 m 15.8 @ 5 m	400 @ 1 m 15.8 @ 5 m
Fluid Flow	Wind, Wave	air: 200-800 water: 500 mW/cm^3	-
Batteries (Lithium) (non-rechargeable)	Electrochemical	89	7
Batteries (Lithium) (rechargeable)	Electrochemical	13.7	0
Fuel Cells (methanol)	Electrochemical	560	56

Scavenging energy from renewable sources for small computing systems is conceptually the best method for extending battery life, and in some cases, achieving batteryless operation [4]. Mechanical movements resulting from ambient vibrations, mobile use of systems, and user interfaces such as keyboards, mice, and trackballs can be considered as such renewable energy sources [5]. Therefore available environmental energy sources are started to be considered as an alternative to batteries. Table 1.1 shows the comparison of power densities of various types of energy sources including batteries and energy harvesting alternatives which is pointing out the long term efficiency of energy harvesting methods with respect to other energy sources [6]. Therefore, the field of energy harvesting is growing both in terms of academic research area and in terms of new commercial products. Recent development in energy harvesting technology shows that environmental energy sources such as heat, light and vibration is able to take place of batteries in near future to charge electronic systems or increase the energy efficiency of the systems by reducing the consumed power. Thus, the growing demand for energy harvesters has motivated the research in this study.

1.2 Energy Harvesting as an Energy Source

Energy harvesting is the conversion of ambient energy (vibration, heat, light) into electrical energy to power small and autonomous electronic devices. For most of the electronic systems, sustainable energy is the most important problem and energy harvesting is the forthcoming solution for energy problems in the next decade. Recent development in energy harvesting technology shows that environmental energy sources have a growing market demand to supply electronic systems shown in Figure 1.1 [7].

Improvements in the low power electronics are an opportunity for energy harvesting technology to be a part of the electronic devices as the power consumption of the electronic systems decrease. Generated power levels is increasing by energy harvesting and power consumption of electronic devices is decreasing which makes the energy harvesting technology feasible and popular to power small electronic systems.

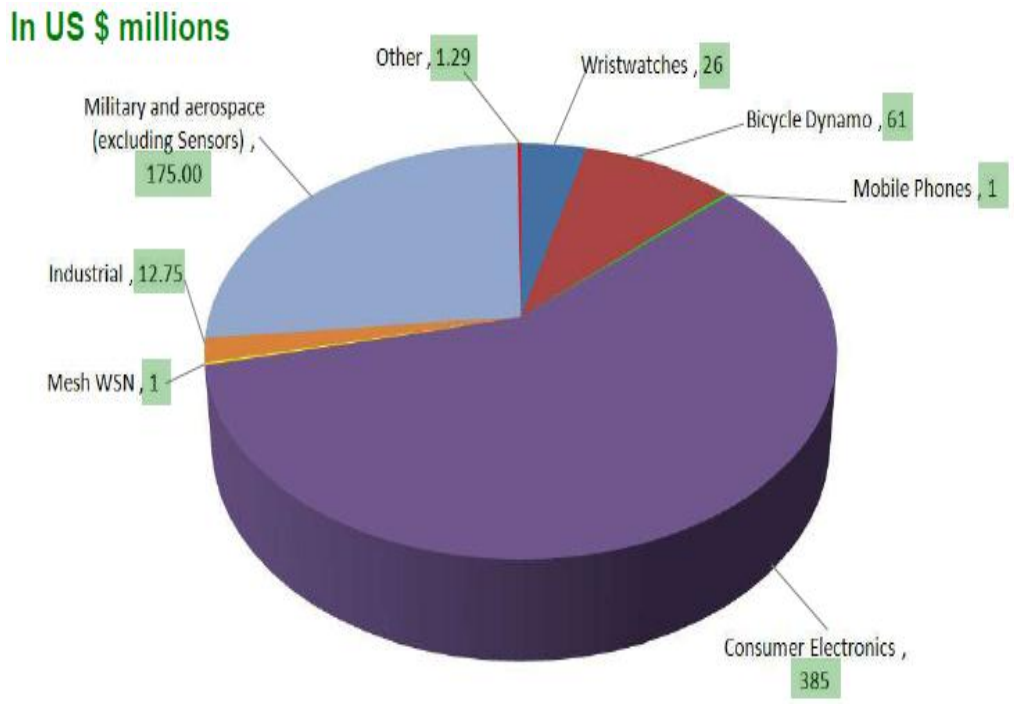

Figure 1.1. Energy harvesting market in 2011 [7].

Most of the electrical and electronic devices are becoming integrated with energy harvesting components so that energy consumption is completely provided by the energy harvesting module or the battery life is extended, increasing the energy efficiency of the system [7]. Figure 1.1 gives a brief information about today's energy harvesting market. The total market value of energy harvesting products is $ 700 million and most of the market is dominated by consumer electronics and military-aerospace applications. According to Figure 1.2, energy harvesting market is expected to reach a market value of $ 4.4 billion in 2020 with a market leader of wireless sensor networks.

Figure 1.3 shows the future trends of the energy harvesting for possible application areas. The dimensions of the devices we are using today are becoming even smaller which arouses the need for smaller energy sources other than batteries. Batteries cannot be integrated into small systems because of their large sizes. Therefore energy harvesting seems to be a solution for supplying power for small autonomous systems. Besides the application area of autonomous systems, energy harvesting will

take place for other systems such as building automation, industrial processes, medical, military, and automotive for today and near future.

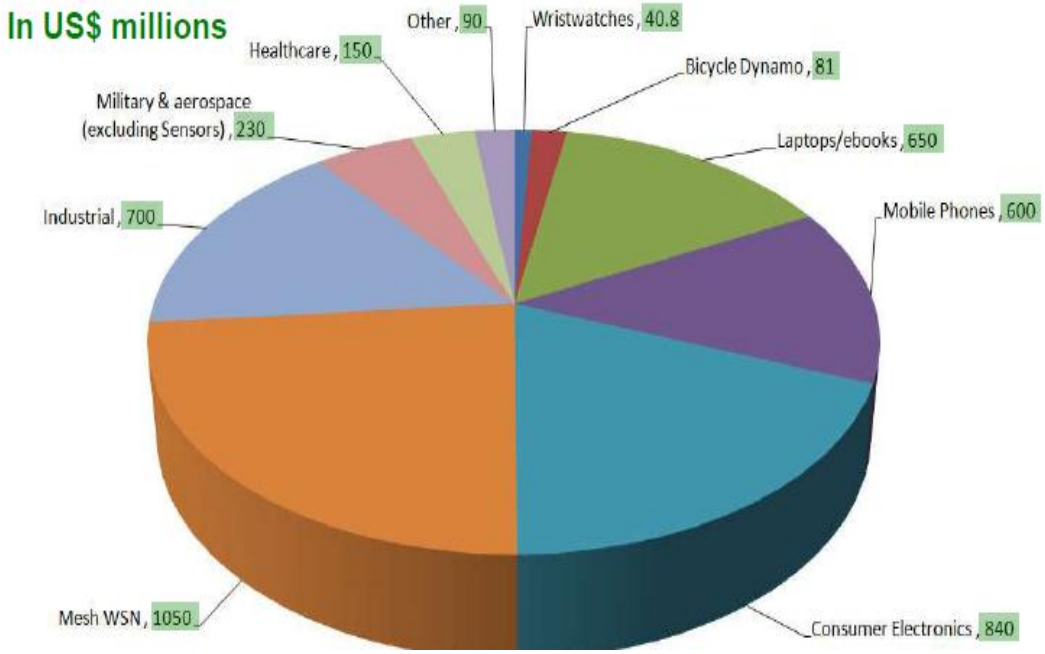

Figure 1.2. Energy harvesting market forecast for 2020 [7].

2010	2012	2014	2020	2024
Devices where size and cost are not too demanding. There are examples within small parts of the sectors: home automation, building automation, industrial processes, medical, military, automotive, road furniture and active radio frequency identification RFID.		A high percentage of home automation, building automation, industrial processes, medical, military, automotive, electronic toys, road furniture, signage, electronic billboards and posters and active radio frequency identification RFID.		
	Integral phone, e-book and laptop chargers such as sprung rollers of photovoltaic film, extended when needed.			
		Energy harvesting e-labels and e-packaging		
			Widespread sensor networks in inaccessible places, including in people, on trees in forest fires, embedded in concrete and dropped on the moon or in battle. Energy harvesting laptops and phones widely deployed in the third world	

Figure 1.3. Timeline for widespread applications of energy harvesting [7].

Furthermore, the only limiting factor for energy harvesting is the working condition of the device or the system on which energy harvesting module will be implemented instead of batteries. Therefore ambient energy source type is the most important parameter for energy harvesting systems. Ambient energy sources are composed of solar energy, waste heat and environmental vibrations. In the scope of this thesis study, environmental vibrations will be investigated for energy harvesting.

1.3 Vibration Based Energy Harvesting

Vibration based energy harvesting is becoming more popular day by day because of the abundance of the environmental vibrations and wide application areas. Some of the vibration sources in the environment are human movements, vehicle motion, common household goods (fridges, washing machines, microwave ovens etc.), industrial plant equipment, moving structures such as buildings and bridges [8]. However, for human power based applications, the vibration frequencies are low while the displacements are large [9, 10]. Due to these characteristics, the scope of this thesis is limited to low frequency vibration energy harvesting with relatively large displacements.

There are three types of vibration based energy harvesting techniques namely: electrostatic, piezoelectric, and electromagnetic energy harvesting. Electrostatic energy harvesting is based on the relative movement of the electrically charged plates of a capacitor with respect to each other, and energy is generated by the change in capacitance and corresponding charge transfer between the plates in response to the external vibrations. Piezoelectric energy harvesting is based on the response of a piezoelectric material to an applied stress. An instantaneous voltage is generated across the piezoelectric material when the stress over the material changes. Electromagnetic energy harvesting is based on the Faraday's Law of electromagnetic induction. Electrical energy is generated by the relative motion between a coil and a magnet. The configuration of the magnet or the coil can be modified to reach higher energy levels according to the application. In the scope of this thesis study, electromagnetic energy harvesting will be discussed in detail.

1.4 Electromagnetic Energy Harvesting

The basic principle in electromagnetic energy harvesting for the generation of electricity is based on the Faraday's law of electromagnetic induction. When an electric conductor is moved along a magnetic field gradient, a current is induced through the conductor, opposing the change in the magnetic field. This results in an emf (electromotive force) across the conductor proportional to the time rate of change of the magnetic flux. Voltage is linked to the flux change and the velocity. In the case of a coil moving in a magnetic field gradient, the induced voltage across the coil is proportional to the magnetic flux change and number of coil turns as given in (1):

$$\varepsilon(t) = -\frac{d\varphi}{dt} = -\frac{d\left(\sum_{i=1}^{n}\left(B.A_i\right)\right)}{dt} \qquad (1.1)$$

where ε is the induced voltage, Φ is the magnetic flux, B is the magnetic field intensity around the coil, A_i is the area of each coil turn, t is time, and n is the total number of coil turns.

Figure 1.4 shows an energy harvesting application of this phenomenon. The harvester is composed of a stationary magnet and parylene cantilevers with planar micro coils fabricated on top [11]. Power is generated through the relative motion of the magnet and the cantilevers.

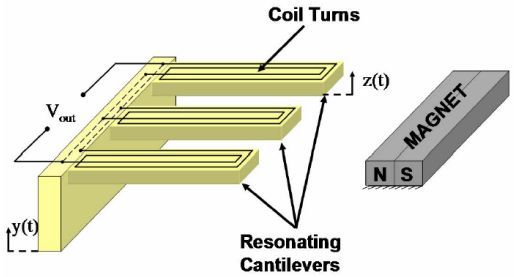

Figure 1.4. Illustration of an electromagnetic harvester [11].

While converting mechanical energy into electrical energy, electromagnetic energy harvesting has advantages over other methods. Electromagnetic energy harvesting is more conformal with micro fabrication steps and no voltage or charge source is required as in electrostatic energy harvesting.

1.5 Review of Electromagnetic Energy Harvesters

Most of the studies in this area exist in centimeter scale where the implementation is quite easier compared to micro scale implementations. However, micro scale studies are also carried out by micro fabrication techniques. The earliest micro scale device was reported by researchers from the University of Sheffield, United Kingdom in 1996 [12, 13]. The device fabrication is achieved in such a way that structures are fabricated on two different wafers and at the end of the fabrication, two wafers are bonded together using silver epoxy. The upper gallium arsenide (GaAs) wafer consists of a circular polymide membrane and the lower wafer has planar integrated coils with 2.5 μm thickness and 5 μm spacing. The device generates 0.3 μW at an operation frequency of 4.4 kHz with an acceleration of 382 m/s^2.

The low power output levels of micro generators have aroused the need for milli scale designs to achieve higher power levels. One of them is proposed by Hami *et al*. in 2000 [14]. Figure 1.5 shows the generator which is composed of a cantilever beam and magnet assembly. The cantilever beam is supported by a housing. There are two magnets placed in opposite direction with each other. This magnet configuration creates a uniform magnetic field through the air gap. The coil is placed in the air gap between the magnets at the right position on the direction of the movement of the mass. As the housing is vibrated, the mass moves relative to the housing, sinusoidally causing the magnetic flux to pass through the coil. This induces an electromotive force on the coil, generating a power level of 0.53 mW within a volume of 240 mm^3 at a vibration frequency of 320 Hz.

As reported above, most of the electromagnetic energy harvesters are designed to operate at high frequencies. This is because of the generation of low power levels at

low frequency vibrations. Nevertheless, there are also some harvesters designed for lower frequencies, achieving moderate power levels. One of them is proposed by Beeby *et al*. in 2007 [15]. The device is a coil-based electromagnetic energy harvester with optimized magnet geometry, which can generate 306 μW/cm^3 at 52 Hz input vibration. The design has four NdFeB magnets on the top and bottom surfaces of a cantilever as shown in Figure 1.6. The arrangement of the magnets produces a concentrated magnetic flux through the stationary coil when the magnets move. This results in an emf (electromotive force) across the conductor proportional to the time rate of change of the magnetic flux.

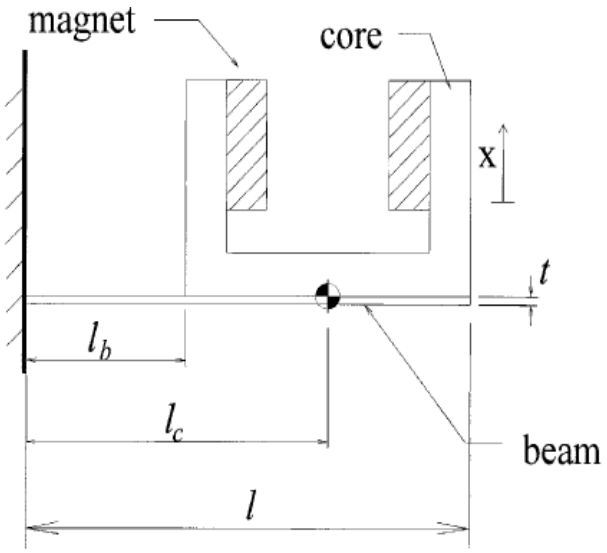

Figure 1.5. Dimensional drawing of beam/magnet assembly [14].

As can be seen from the above examples, in vibration based energy harvesting, the generator is exposed to external vibrations and this results in a position change between a magnet and a coil, leading to an induced voltage. However, the resonance frequency of the generator should match with the natural frequency of the external vibrations for maximum energy extraction. Otherwise, the generator movement is limited in response to external vibrations. To solve this problem, some generators are designed in a way to work within a range of frequencies, and these are referred as wideband generators.

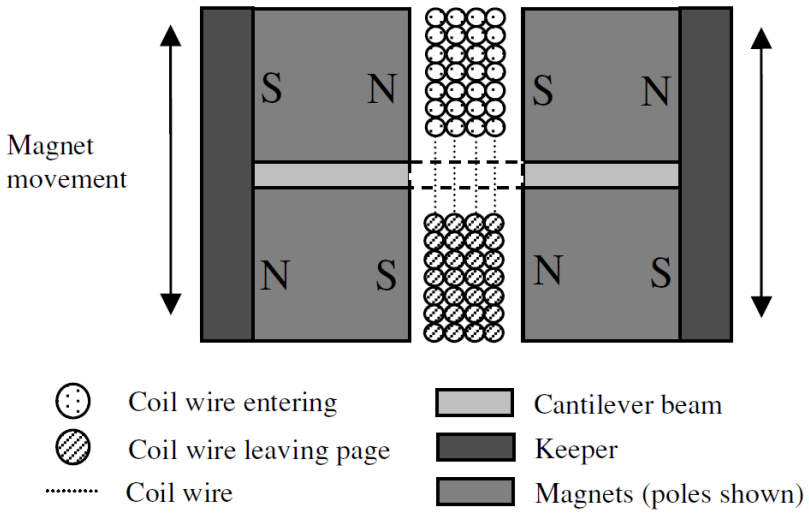

Figure 1.6. Cross section of an EM energy harvester operating at 53 Hz [15].

One of these generators is proposed by Ching *et al.*, a multimodal resonant energy harvester with a total volume of 1 cm^3 generating a maximum power of 830 μW at frequencies ranging from 60 to 110 Hz [3]. The generator works in a wide range of external vibrations to drive low power ICs or micro sensors. The generator consists of a NdFeB magnet, springs and coil turns. The spring is attached to the magnet and a solid frame. The electrical coil is fixed on the rigid housing. When the rigid housing vibrates with external vibrations, the magnet moves relatively to the coil with three different modes of resonant vibration. The varying amount of magnetic flux passing through the coils induces a voltage on the coils.

Another wideband vibration energy harvester is proposed by Sari *et al*. in 2008, at which the micro generator is capable of generating power over a predetermined frequency range [16]. Power is generated by means of the relative motion between a magnet and coil turns fabricated over resonating cantilevers. Figure 1.7 shows the wideband operation of the device which is obtained by the implementation of cantilevers with different lengths with varying natural frequencies.

As the resonance frequency of the vibration based energy generators decreases, generator volume starts increasing due to large mass requirements to lower the operation frequency. This requirement causes an increase in the magnet dimensions,

resulting in higher magnetic field strengths which enable higher generated voltage levels. As a result, achieving higher voltage levels at low frequencies by larger magnet configurations enlarges the overall volume of the generator. Therefore, at low frequencies, mostly centimeter scale generators exist in the literature. One of them is proposed by Amirtharajah *et al*. in1998, an electromagnetic energy harvester with a power density level of 17 μW/cm^3 operating at 2 Hz vibration frequency [17]. A moving coil electromagnetic transducer was used as power generator and a power level of 400 μW is expected according to calculations. Another low frequency generator is developed by Nakano *et al*. in 2002, with a moving magnet that delivers 150 μW/cm^3 at 2 Hz vibration frequency [18]. In another study, with a vibration energy harvester that is able to harvest energy from self-excited rotation, 190 μW/cm^3 power density at 6 Hz vibration frequency was reported by Sasaki *et al*.

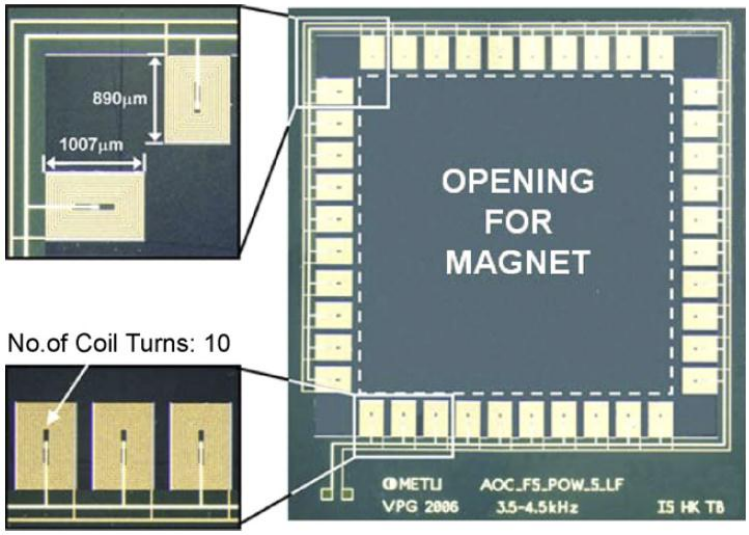

Figure 1.7. Wideband electromagnetic generator [16].

Apart from the generators listed above, a novel method, called frequency up-conversion, up-converting the low frequency vibrations to a higher frequency to generate power through electromagnetic induction has been proposed by Külah and Najafi [19]. In this method, topology consists of a low frequency magnet diaphragm and high frequency cantilevers on which coils are fabricated.

In this structure, a magnet diaphragm holds a NdFeB magnet for both frequency up-conversion and power generation through electromagnetic induction. The diaphragm-magnet assembly resonates in response to vibrations of 1 Hz. The cantilevers have coil turns for induction, and a higher induced resonance frequency. Also, at the tip of the cantilevers, magnetic actuation area exists for interaction with the magnet. The distance between magnet and the cantilevers is optimized such that the magnet catches the cantilever at some point during movement, pulls them up, and releases at another point. The released cantilevers starts resonating at their damped natural frequencies, realizing the frequency up-conversion, hence increasing the energy harvesting efficiency. The reported energy harvester prototype has a power density of 0.05 $\mu W/cm^3$ within a practical prototype volume of about 2.3 cm^3, operating at 1 Hz input vibration frequency. A microfabricated version of this device is also reported by Sari *et al*. in 2008 (Figure 1.8) [20], generating a power of 0.25 nW per cantilever, up-converting the vibrations at a frequency range of 100 Hz.

Although, the micro fabricated version of the frequency up-conversion mechanism has an impact in the literature by converting low frequency vibrations to high frequency vibrations, thus enhancing the possibility of working in low frequency environments, the generated power level still needs improvement. The main reason for this low power level is the low number of coil turns (due to insufficient area) in each cantilever and high resistance (due to low thickness) of coil turns. Each cantilever has 6 coil turns having a thickness of 0.1 μm decreasing the available power level. Another important factor that results in the low output power is the synchronization problem of the different cantilevers.

The device is composed of 20 cantilevers, but integrating 20 consecutive cantilevers into the first generation module, depicted in Figure 1.8, did not yield proportionate scaling of the output power compared to a single cantilever. This was due to the variation between the natural frequencies of the cantilevers, and not perfectly synchronized catch and release moments of the cantilevers, which resulted in phase shifts across the cantilever outputs, reducing the available aggregate power.

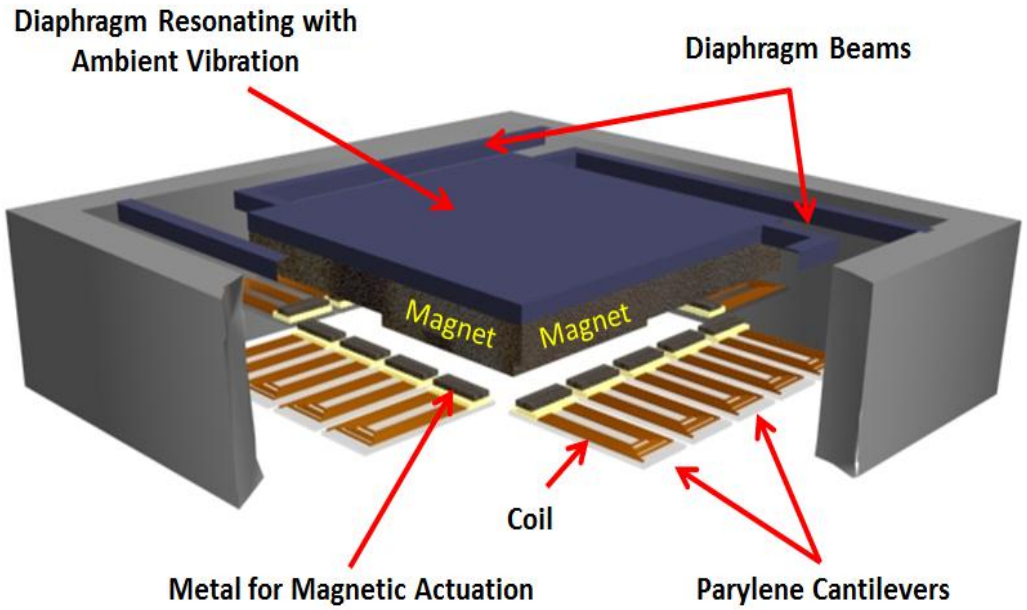

Figure 1.8. First generation frequency up-conversion design [20].

The first generation frequency up-conversion design has the following problems;

1. Insufficient area (1000 x 430 μm^2) for coil turns, resulting a total number of 6 coil turns on each cantilever,
2. Low number of coil turns on each cantilever, resulting in the generation of low voltage levels,
3. High coil resistance due to low coil thickness, decreasing the generated power levels,
4. Variation between the natural frequencies of the cantilevers, causing phase shifts across the cantilever outputs and synchronization issues, reducing the available aggregate power.

1.6 Objective of the Thesis Study

The aim of this thesis study is to improve the energy efficiency of the first generation electromagnetic frequency up-conversion design described above at low frequency environmental vibrations.

The proposed new architecture focuses on the following goals;

1. Increase the coil area, hence the number of coil turns to achieve the desired voltage levels,
2. Decrease the coil resistance by implementing thick coil layers so that generated power level is increased,
3. Eliminate and solve the phase shift and synchronization problem across the cantilevers.

In order to achieve the above objectives, the following steps are planned to be realized.

1. Modeling and design of a monolithic diaphragm based frequency up-conversion architecture.
2. Mechanical design and analysis of the proposed design in Comsol® Multiphysics® for proper operation.
3. Development of an automation engine for the analysis of the performance parameters.
4. Simulation of finalized design in Matlab® Simulink® and in the development tool (automation engine).
5. Fabrication and testing of the proposed design in macro scale for proof of concept.
6. Fabrication and testing of the proposed design in micro scale.

1.7 Outline of the Thesis

In the first chapter, energy harvesting alternatives have been discussed and the focus has been given to vibration based energy harvesters. Following this, a detailed review of electromagnetic energy harvesters has been presented. This is followed by the statement of objectives and aims of the study.

In the second chapter, a new frequency up-conversion method has been proposed to accomplish the objectives of the thesis. Mathematical analysis, mechanical design and related modeling and simulation results have also been presented in this chapter.

Following the modeling and simulation, Chapter 3 presents the macro scale prototyping of the proposed micro generator structure. Fabrication steps of the macro prototype have been explained and experimental results have also been discussed in this chapter.

Chapter 4 deals with the detailed micro fabrication procedure of the proposed micro generator. Microfabrication steps of the generator have been explained in this chapter.

Finally, chapter 5 presents concluding remarks and future work recommendations.

CHAPTER 2

THEORY, DESIGN AND SIMULATIONS OF THE LOW FREQUENCY ELECTROMAGNETIC ENERGY HARVESTER

This chapter presents the theory, design and simulation of the second generation frequency up-conversion design. Firstly, Section 2.1 discusses the design properties and advantages of the proposed frequency up-conversion design, and it presents solution approaches for improving the cantilever based design shown in Figure 2.1. Section 2.1.1 and 2.1.2 describes various types of monolithic diaphragms as an alternative to cantilevers. Afterwards, the appropriate diaphragm design has been selected considering the available area for coil turns and displacement amounts. The mechanical modeling of the diaphragms and simulations are performed in Comsol® Multiphysics® environment in these sections. After the selection of the suitable diaphragm for proper operation, Section 2.2 presents detailed mathematical model, analysis, and related simulation results. For measuring the performance of the design in response to different design parameters, a user interface based development tool has been built up in Visual® Basic® environment. Section 2.3 explains the details of this development tool which takes design and excitation parameters as input, and estimates output voltage waveforms and power levels. The chapter is finalized with the performance results of the proposed generator.

In the new design, a diaphragm structure exists instead of cantilevers on which micro coils are fabricated. The magnet diaphragm is excited by low frequency environmental vibrations. Magnet diaphragm starts resonating in response to these vibrations and catches and releases the lower high frequency coil diaphragm. After the release, the coil diaphragm starts resonating at its own damped natural frequency. Voltage is generated by the relative motion of the coil diaphragm with respect to the magnet.

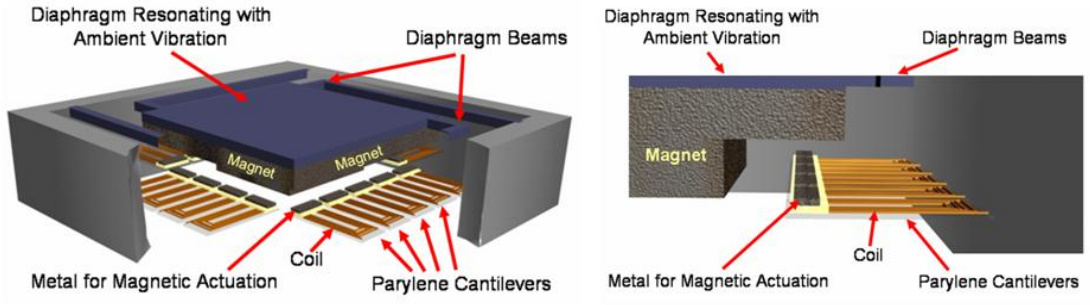

Figure 2.1. First generation frequency up-conversion design [20].

2.1 The proposed frequency up-conversion structure

Figure 2.2 shows the proposed frequency up conversion structure. The structure consists of an upper and a lower diaphragm (Figure 2.3), having different resonance frequencies. The upper diaphragm holds a NdFeB magnet both for frequency up-conversion and power generation through electromagnetic induction. The diaphragm-magnet assembly resonates with vibrations in the range of 1-100 Hz. The lower diaphragm has coil turns for induction, and a higher induced resonance frequency of 2-3 kHz. Also, in the middle of the lower diaphragm, magnetic film is formed for interaction with the magnet. The distance between the diaphragms is optimized such that the magnet catches the lower diaphragm at some point during movement, pulls up, and releases at another point. The released lower diaphragm then starts resonating at its damped natural frequency with the given initial condition, and hence up converts frequency of vibrations. The motion of the released diaphragm exponentially decays out, but the cycle restarts before the induced vibration dies.

The proposed design shown in Figure 2.2, improves the performance of the cantilever based first generation frequency up-conversion design by using a monolithic diaphragm instead of cantilevers, increasing the available area for implementation of maximum number of coil turns.

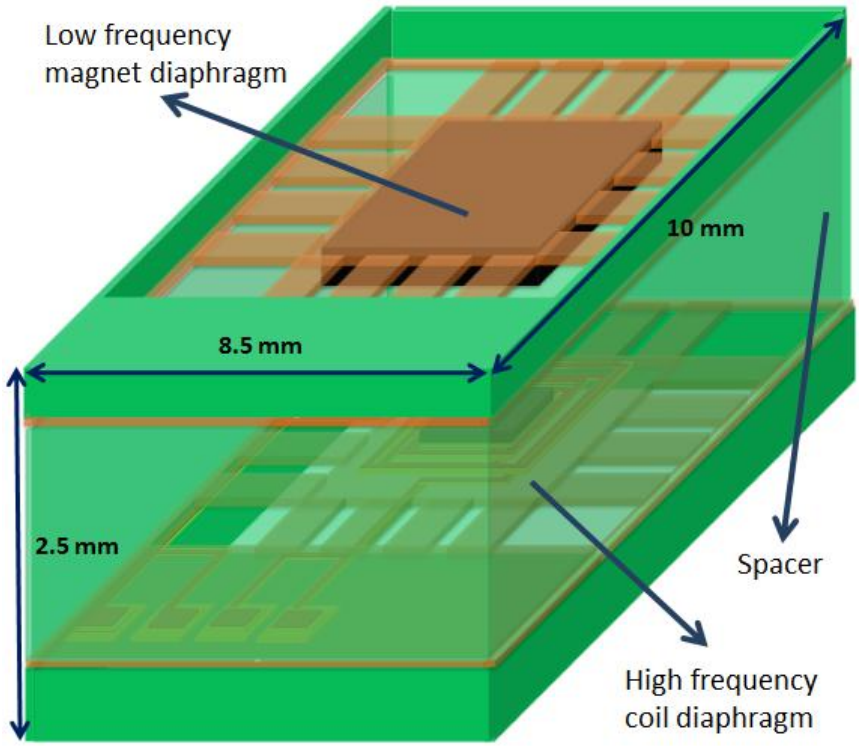

Figure 2.2. Schematic view of the proposed frequency up-converter (FUC) design.

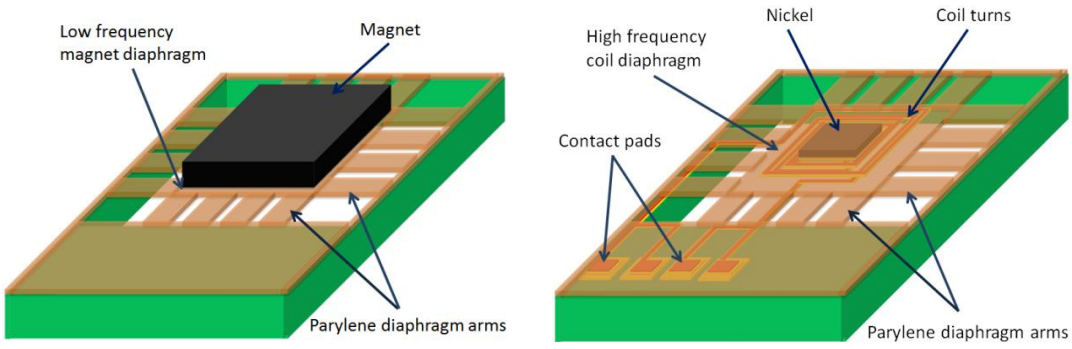

Figure 2.3. Low frequency magnet diaphragm (left), high frequency coil diaphragm (right).

2.1.1 The design of the lower diaphragm

After explaining the whole structure and the proposed new frequency up-conversion design with two diaphragms, the design and the mechanical structure of the lower diaphragm can be presented. Structure of the diaphragm is an important performance parameter for the whole design, considering the factors such as maximization of available area for coil turns, achieving the vertical displacement during the motion and realizing reliable operation. Within the scope of designing a monolithic diaphragm instead of cantilevers, mechanical models have been developed for different diaphragm types.

These diaphragm types have been modeled in Comsol® Multiphysics® environment, considering the dimension restrictions for MEMS design and packaging, allowing an available area of 10 x 8.5 mm^2. This is followed by the mechanical simulations testing the vertical motion of the diaphragms, indicating to be an appropriate candidate as a lower diaphragm for frequency up-conversion mechanism.

Alternative diaphragm designs studied in this work are shown in Figure 2.4-6. The first diaphragm type shown in Figure 2.4 has a high displacement amount vertically in z direction, resulting in high voltage levels by the high rate change of the magnetic flux lines through the coils on the diaphragm. However, the proposed diaphragm has more than one mode shape within close frequency values, resulting motion in x and y direction which is not appropriate for the frequency up-conversion mechanism. This problem has been solved in the second alternative design presented in Figure 2.5 by using stiff and rectangular shaped arm structures. However, considering the need for a large area for the coil turns, second alternative is also eliminated. Therefore, the requirements of vertical motion in z direction and a large area for maximum coil turns have aroused the need for another design. The third design shown in Figure 2.6 has been developed in order to satisfy the requirements for larger area (3.8 x 3.8 mm^2), allowing the implementation of high number of coil turns (96 turns), while retaining a significant amount of motion in the z-direction.

2.1.2 Mechanical Modeling of the Diaphragm

After the discussion and determination of the most suitable diaphragm type, the optimization of the diaphragm parameters is studied. This includes the investigation of the mechanical design parameters such as structural material properties, dimensions of the diaphragm and the diaphragm arms, the number of arms attached to the diaphragm structure which affects overall stiffness, natural frequency, and the displacement amount of the structure.

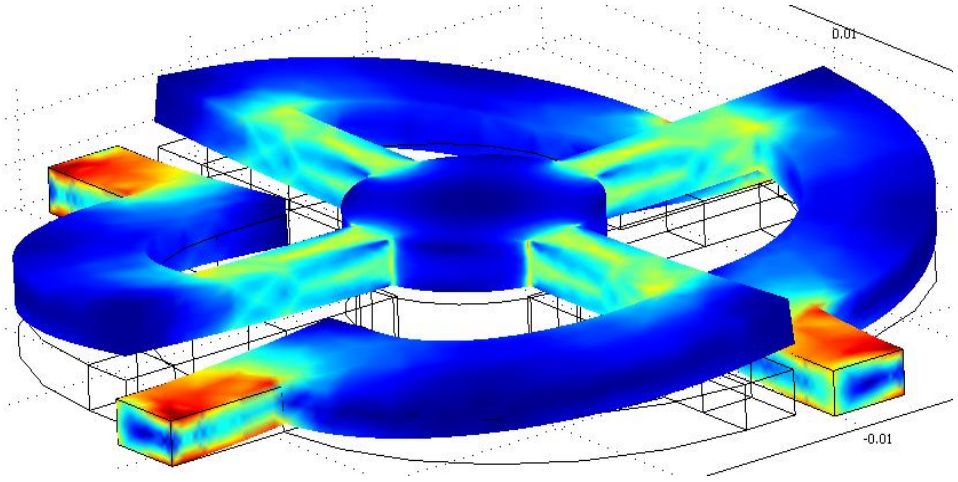

Figure 2.4. First alternative design for coil-diaphragm.

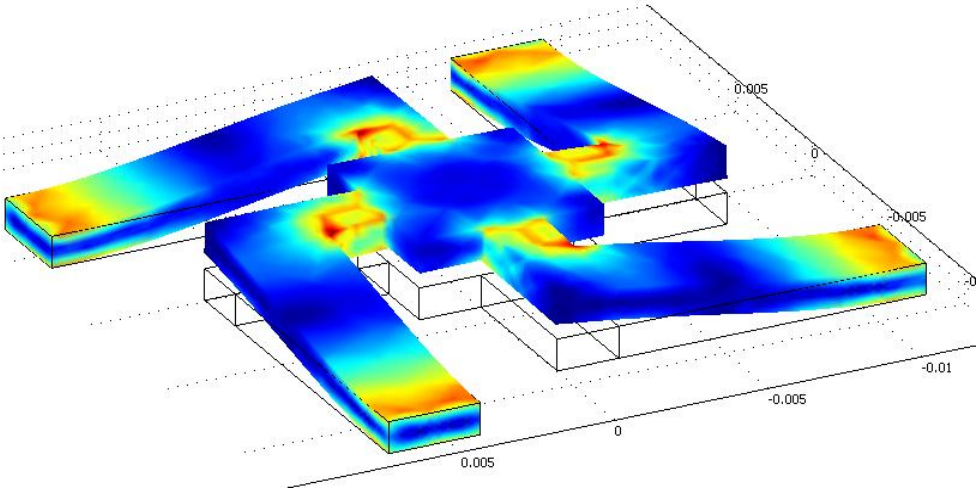

Figure 2.5. Second alternative design for coil-diaphragm.

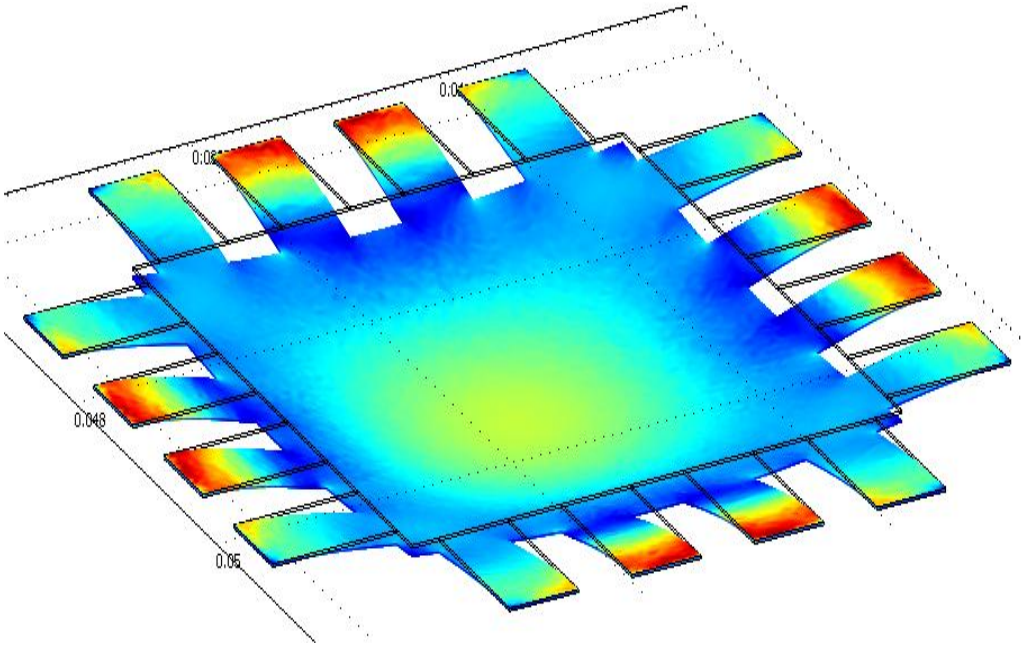

Figure 2.6. Third alternative design for coil-diaphragm.

In this study, Parylene C is used as the structural material for the diaphragms. The reason for selecting Parylene C is its high reliability for large deflections in response to vibrations [4]. The thickness of the parylene is adjusted in such a way that desired natural frequency values are obtained for the diaphragms. This is critical for the dynamic system performance especially for the frequency up-conversion technique. Therefore, in this part determining the natural frequency of the diaphragms will be discussed.

The natural frequency of the diaphragms can be calculated as:

$$w_n = \sqrt{\frac{k_{eq}}{m_{eq}}} \tag{2.1}$$

where k_{eq} is the equivalent stiffness of the diaphragm arms and m_{eq} is the equivalent mass of the diaphragm. In order to calculate k_{eq}, the stiffness of each arm should be calculated. The stiffness of a rectangular fixed-fixed beam can be used for this calculation:

$$\left(k_{eq}\right)_{\substack{single\\arm}} = \frac{192EI}{(2L)^3} = \frac{24EI}{L^3} \tag{2.2}$$

where E, I and L are the modulus of elasticity, area moment of inertia and length of each arm. Then, for 8 arms connected in parallel, the stiffness equation can be defined as,

$$k_{eq} = 8\left(k_{eq}\right)_{\substack{single\\arm}} = \frac{192EI}{L^3} \tag{2.3}$$

The equivalent mass lumped at the midpoint for a fixed-fixed beam with mass "2m" can be determined as:

$$m_{eq} = \frac{13}{35}(2m) = 0.37(2m) = 0.74m \tag{2.4}$$

For the coil diaphragm, since there are 8 arms, a magnetic actuation material (nickel), and coil turns, the total equivalent mass becomes,

$$m_{eq} = 5.92m + M_{nickel} + M_{coil} \tag{2.5}$$

The mass of the nickel film can be expressed as follows;

$$M_{nickel} = a_n \times b_n \times c_n \times \rho_{nickel} \tag{2.6}$$

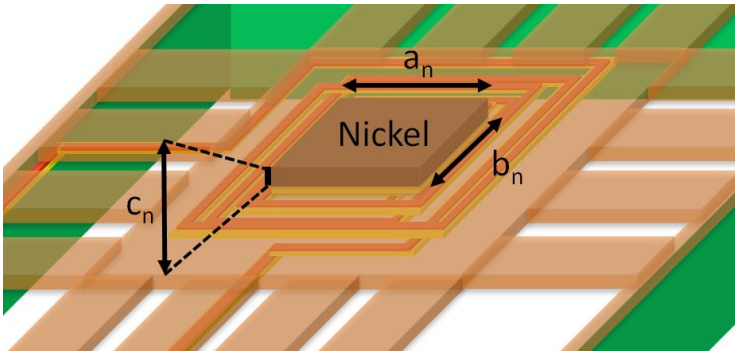

Figure 2.7. Magnetic actuation area for magnetic actuation.

The mass of the coil turns are:

$$M_{coil} = L \times w \times t \times d_{coil} \tag{2.7}$$

where L stands for the total length of the coil, w is the width of the coil, t is the thickness and d is the density of the coil material as shown in Figure 2.8.

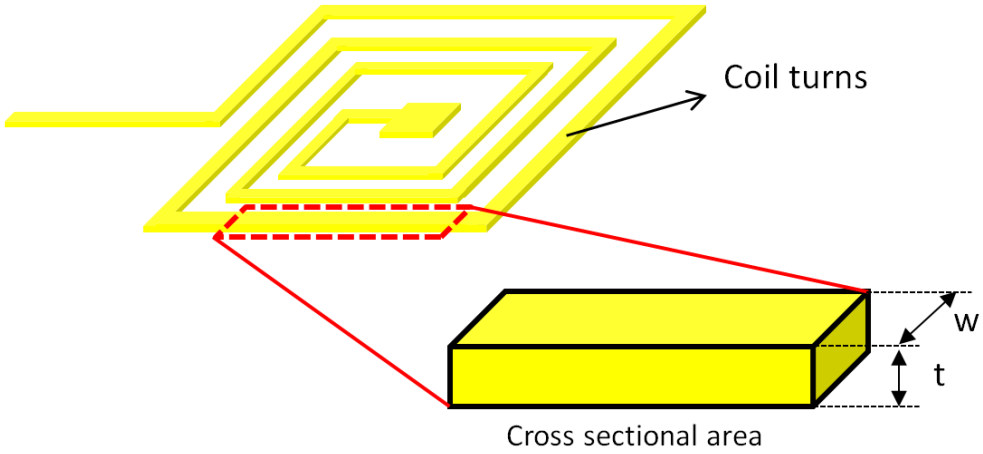

Figure 2.8. Cross-sectional area of rectangular coil.

As a result for the coil-diaphragm, the natural frequency becomes:

$$w_n = \sqrt{\frac{k_{eq}}{m_{eq}}} = \sqrt{\frac{192EI}{(5.92m + M_{nickel} + M_{coil})L^3}} \tag{2.8}$$

For the magnet diaphragm, magnet mass should be considered in the calculation of natural frequency of the diaphragm. Since there are 8 arms and a magnetic mass, M_{magnet}, the total equivalent mass becomes,

$$m_{eq} = 5.92m + M_{magnet} \tag{2.9}$$

As a result for the magnet-diaphragm, the natural frequency of the first bending mode is,

$$w_n = \sqrt{\frac{k_{eq}}{m_{eq}}} = \sqrt{\frac{192EI}{(5.92m + M_{magnet})L^3}} \tag{2.10}$$

2.2 Modeling and Simulation

Following the simulations and mechanical design, a mathematical model for the induced voltage and power is constructed. Afterwards, equation of motion for the diaphragms is developed and mechanical properties and necessary equations are obtained for the dynamic model of the system.

The basic electrical model for the high frequency coil diaphragm is shown in Figure 2.9. The power delivered to the load resistance through the coil is:

$$P = \frac{1}{2} i^2 R_L \tag{2.11}$$

where R_L is the equivalent load resistance of the electrical circuitry. The current induced through the coil, denoted as i, can be defined through,

$$i = \frac{\varepsilon}{R_L + R_C} \tag{2.12}$$

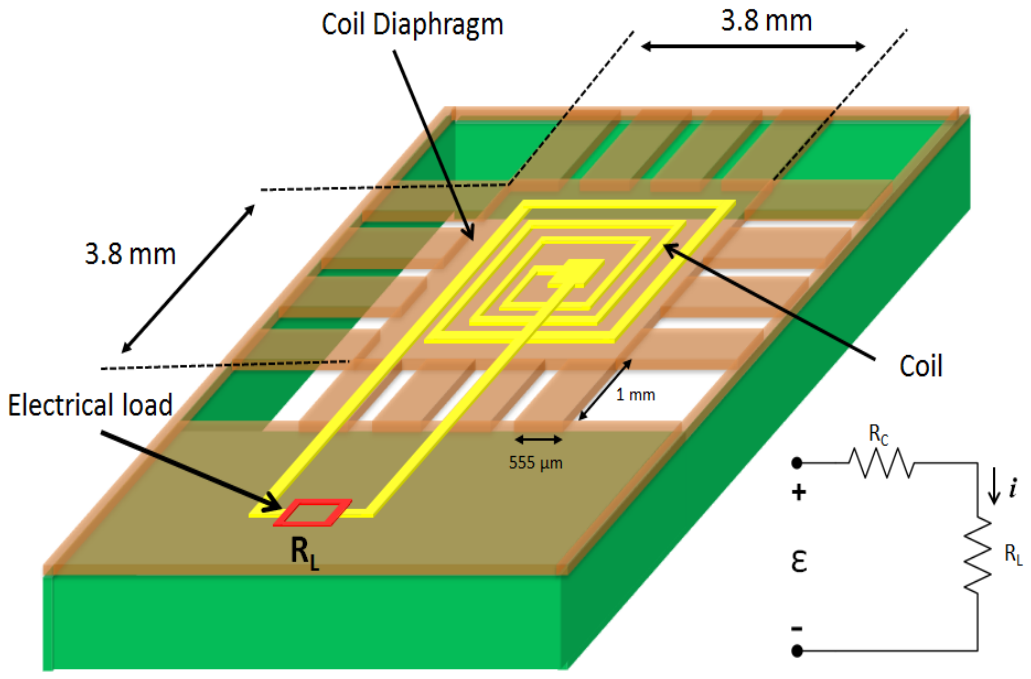

Figure 2.9. Basic electrical model of a coil driving a resistive load.

In this equation, R_c is the coil resistance and R_L is the resistive load driven by the coil.

The resistance of the a rectangular cross sectioned coil is defined by;

$$R_C = \rho \frac{L}{A} \tag{2.13}$$

where ρ is the resistivity of the coil material, L is the length and A is the cross sectional area of the coil. ε is the total induced voltage across the coil according to the Faraday's Law of Induction, and can be expressed as:

$$\varepsilon = -\frac{d\Phi}{dt} = -\frac{dB}{dz}\frac{dz}{dt}\sum_{i=1}^{n} A_i \tag{2.14}$$

where Φ is the magnetic flux, A_i is the area of the each coil turn, B is the magnetic field intensity across the coil produced by the magnet, which can be calculated as:

$$B(z) = \frac{B_r}{\pi}\left(\operatorname{atan}\left(\frac{a_1 a_2}{2z\sqrt{a_1^2 + a_2^2 + 4z^2}} \right) - \operatorname{atan}\left(\frac{a_1 a_2}{2(z+d)\sqrt{a_1^2 + a_2^2 + 4(z+d)^2}} \right) \right) \tag{2.15}$$

where a_1, a_2 and d are the magnet dimensions, B_r is the residual magnetic flux density, and z is the distance from the magnet.

After obtaining suitable expressions for induced voltage, area of each coil turn, and magnetic field, B, the relative velocity term, dz/dt should be determined. For this purpose a suitable mechanical model should be constructed.

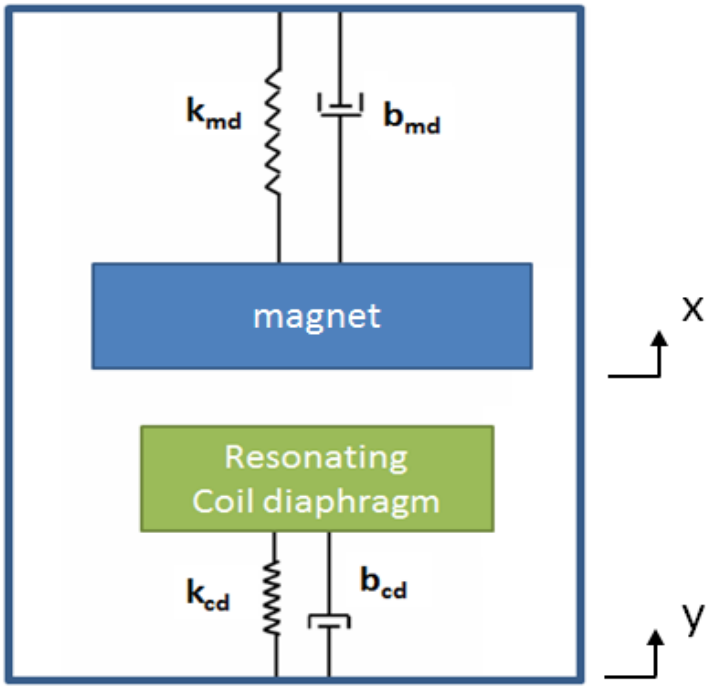

Figure 2.10. Equivalent mechanical model of the dynamic system.

Environmental vibrations excite the mechanical structure of the system shown in Figure 2.10. Displacement of the whole system is defined as "y" and displacement of the magnet in response to excitation is defined as "x". The diaphragm-magnet assembly resonates with vibrations in the general range of 1-100 Hz in response to the environmental vibrations and catches the lower diaphragm, pulls up, and releases it at some point. The released lower diaphragm then starts resonating at its damped natural frequency with the given initial condition. The motion of the released diaphragm exponentially decays out, but the cycle restarts before the induced vibration dies. The natural frequency of the coil diaphragm is designed as to be much higher than the frequency of environmental vibrations so that environmental vibrations do not affect the motion of coil diaphragm. In this model, the dynamic behavior of the magnet diaphragm [21] can be defined as:

$$m_{md}\ddot{z}_{md} + b_{md}\dot{z}_{md} + k_{md}z_{md} = -m_{md}\ddot{y} \tag{2.16}$$

The resulting steady-state behavior of the magnet diaphragm can be represented by the following equation.

$$z_{md}(t) = \left| \frac{m_{md} w^2 Y}{-m_{md} w^2 + jwb_{md} + k_{md}} \right| \sin(wt) \tag{2.17}$$

where z_{md} is the relative displacement of the magnet with respect to the base, m_{md} is the mass of the magnet, k_{md} is the equivalent stiffness of the magnet diaphragm, b_{md} is the equivalent damping constant for the magnet diaphragm and ς_{md} is the damping ratio of the magnet diaphragm.

The dynamic behavior of the high frequency coil diaphragm [21] is given by:

$$m_{cd}\ddot{z}_{cd} + b_{cd}\dot{z}_{cd} + k_{cd}z_{cd} = 0 \tag{2.18}$$

Because the natural frequency of the coil diaphragm is much higher than the environmental vibrations, it is assumed that environmental vibrations do not affect the movement of coil diaphragm. In the final equation, z_{cd} is the relative displacement of the coil-diaphragm with respect to the base, m_{cd} is the equivalent mass, k_{cd} is the equivalent stiffness, b_{cd} is the equivalent damping constant and ς_{cd} is the damping ratio of the coil diaphragm.

The relative displacement of the coil diaphragm with respect to the base, z_{cd} can be obtained by solving the above equation with the initial conditions [21]. As a result, using Laplace transformation the relative velocity of the coil diaphragm is obtained as:

$$\dot{z}(t) = -z_0 w_n \frac{e^{-\zeta_{eq} w_n t}}{\sqrt{1-\zeta_{eq}^2}} \sin(w_d t) \tag{2.19}$$

where z_0 is the initial displacement imposed on the coil diaphragm, w_d and w_n are the damped natural and natural frequencies of the coil diaphragm, respectively. ζ_{eq} is the equivalent damping ratio of the system.

As a result, when only the initial conditions are considered the output voltage generated by the coil diaphragm is:

$$\varepsilon = -\frac{d\Phi}{dt} = \frac{dB}{dz} z_0 w_n \frac{e^{-\zeta_{eq} w_n t}}{\sqrt{1-\zeta_{eq}^2}} \sin(w_d t) \sum_{i=1}^{n} A_i \tag{2.20}$$

and power term can be expanded as:

$$P = \frac{1}{2} \left(\frac{\dot{B} z_0 w_n \frac{e^{-\zeta_{eq} w_n t}}{\sqrt{1-\zeta_{eq}^2}} \sin(w_d t) \sum_{i=1}^{n} A_i}{R_L + R_C} \right)^2 R_L \tag{2.21}$$

In the equations above, w_d is the damped natural frequency of the coil diaphragm defined by,

$$w_d = w_n \sqrt{1-\varsigma_{eq}^{\ 2}} \tag{2.22}$$

Up to this point, the diaphragms are modeled for their separate motion independent of each other. However, due to the operation principle, the system actually has two operation modes: (i) the separate motion at which the magnet and coil diaphragm move separately and (ii) the combined motion at which they move together. The contact force obtained from the governing equation [21] for the combined motion can be defined as follows,

$$T = m_{md}(\ddot{z} + \ddot{y}) + b_{md}\dot{z} + k_{md}(z - \delta_{md}) \tag{2.23}$$

For the combined motion, contact force should be larger than the magnetic attraction force, and magnetic attraction force needs to be larger in order to make diaphragms move separately. This condition can be represented as follows:

Combined motion $T > -F_m$
Separate motion $T < -F_m$ (2.24)

T is the contact force between the bodies and F_m is the magnetic attraction force between the diaphragms during contact and it is defined by,

$$F = \frac{B^2 A_m}{2\mu_0} \tag{2.25}$$

where B is the magnetic field density defined previously, A_m is the magnetic contact area, and μ_0 is the permeability of free space [21].

With these equations, the analytical modeling of the proposed structure can be done. In order to be able to simulate many conditions in a systematic way, a development tool is designed, based on these equations. This will be explained in the following section.

2.3 Development Tool

For predicting the performance of the proposed design in response to different design parameters, a user interface based development tool has been built up in Visual® Basic® environment. Figure 2.11 shows the tool output from the energy harvester module. The tool includes the automation of the physical equations and additional modeling capabilities to achieve simulation accuracy for the generator performance, while accommodating improvements in the design topology studied in this work with respect to the previous study [20]. The tool takes design and excitation parameters as input, and estimates output voltage waveforms and power levels.

The evolution of the energy harvesters from first to second generation is a good example of such design advancement. For example, empirical measurement based miscorrelation factors due to material and fabrication tolerances as well as measurement errors have been integrated into the development tool. The correlation factors have been established after the validation of the first generation MEMS module. In addition, the tool can accommodate topology changes with minimum incremental effort.

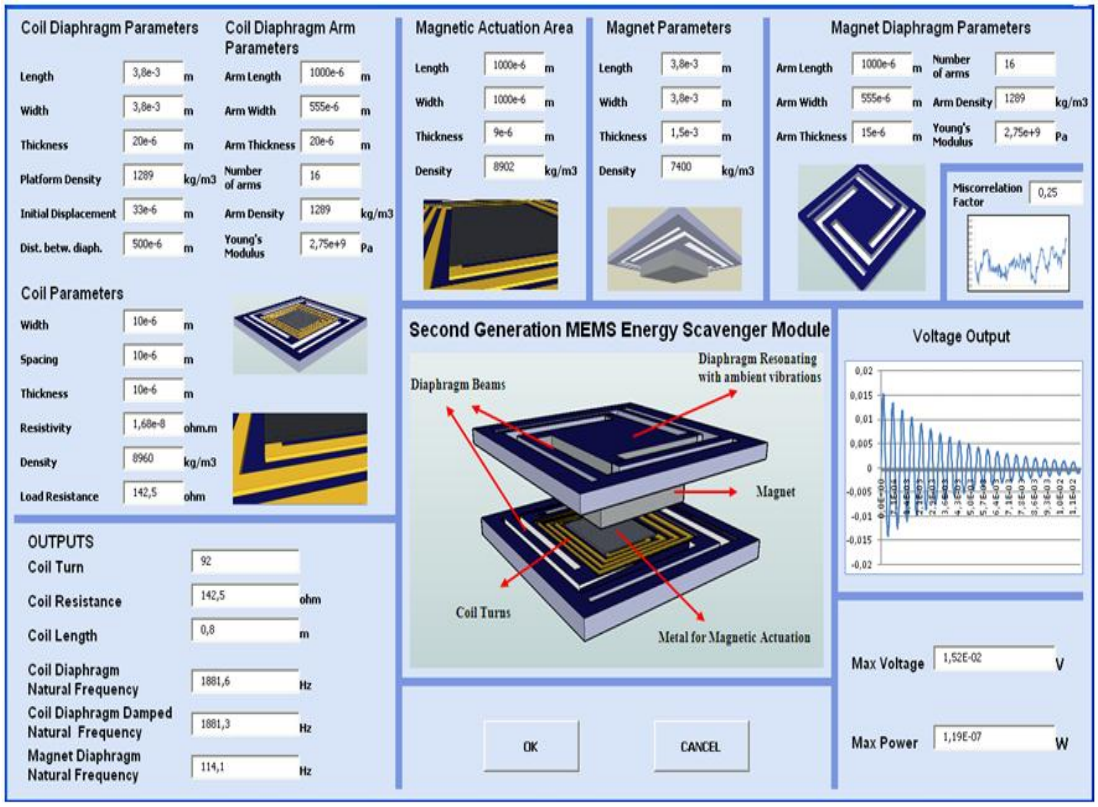

Figure 2.11. Development tool for estimating power output from the second generation MEMS energy harvester module.

While calculating the voltage and power outputs, the most important parameter is the release height of the coil diaphragm. This parameter is calculated in Simulink® environment and all other parameters of the generator are justified in order to maximize the release height of the coil diaphragm. Release height of the diaphragm is directly related to the mechanical structure and design of the diaphragm (Figure 2.12), magnetic actuation area and the strength of the magnet (Figure 2.13). As discussed previously, diaphragm design has been determined in such a way to maximize the area for coil turns and maximize the displacement in z direction at the same time. Following this design, magnetic actuation area is the next important parameter affecting the release height of the diaphragm. Figure 2.14 and Figure 2.15 show the release height of the lower diaphragm with respect to different magnetic actuation area values.

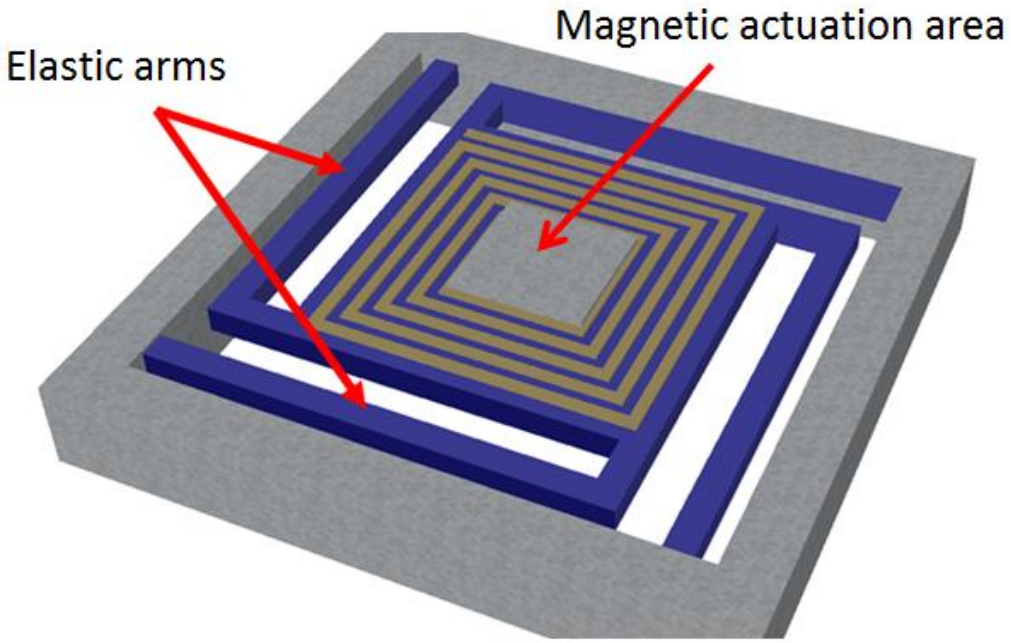

Figure 2.12. Mechanical structure of the coil diaphragm.

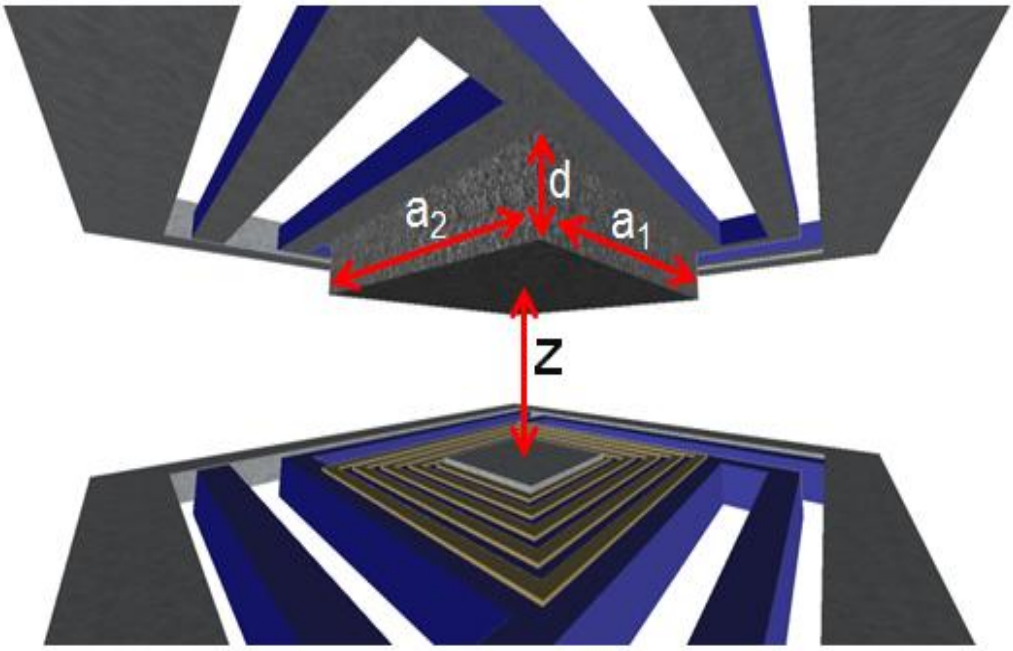

Figure 2.13. Schematic drawing of the magnet diaphragm together with the coil diaphragm.

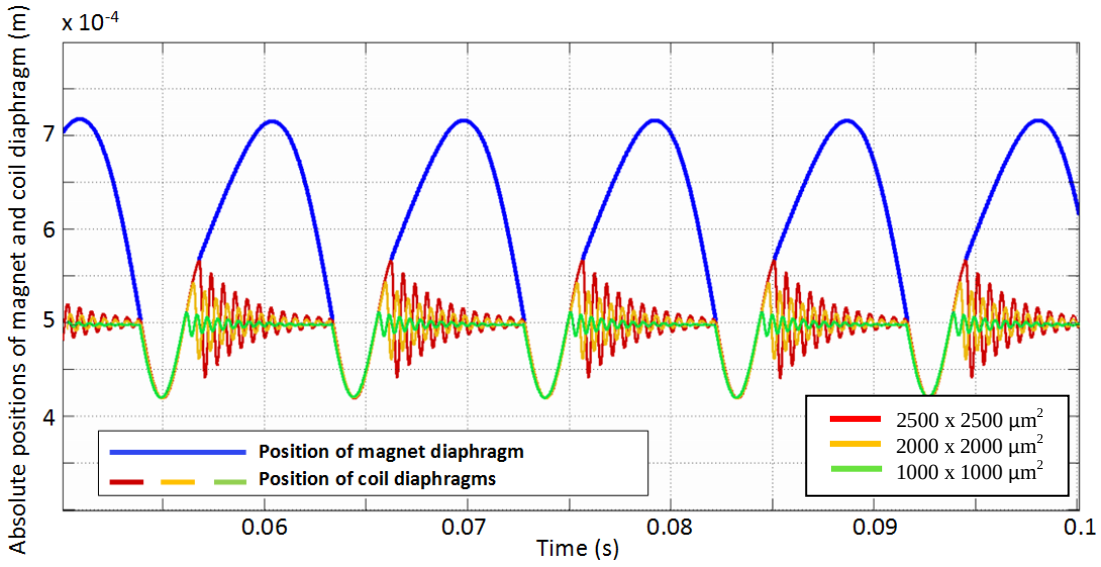

Figure 2.14. Absolute positions of the magnet and coil diaphragm with varying magnetic actuation area.

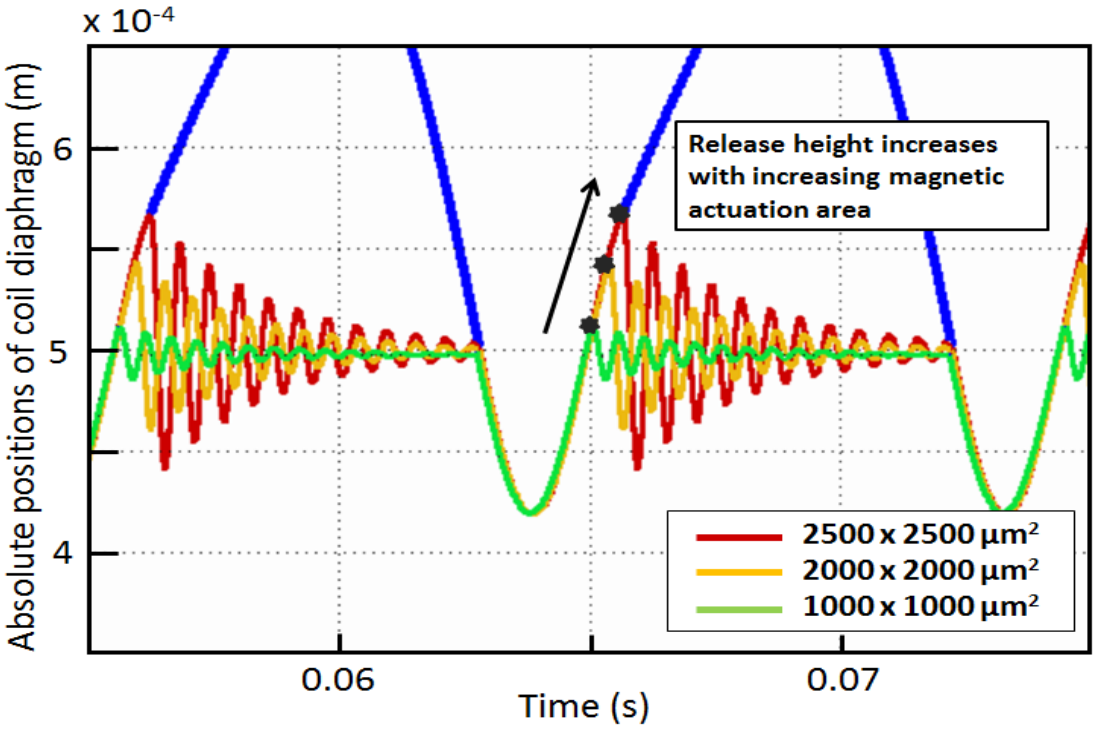

Figure 2.15. Relationship between magnetic actuation area and release height of coil diaphragm: a close-up view of Figure 2.14.

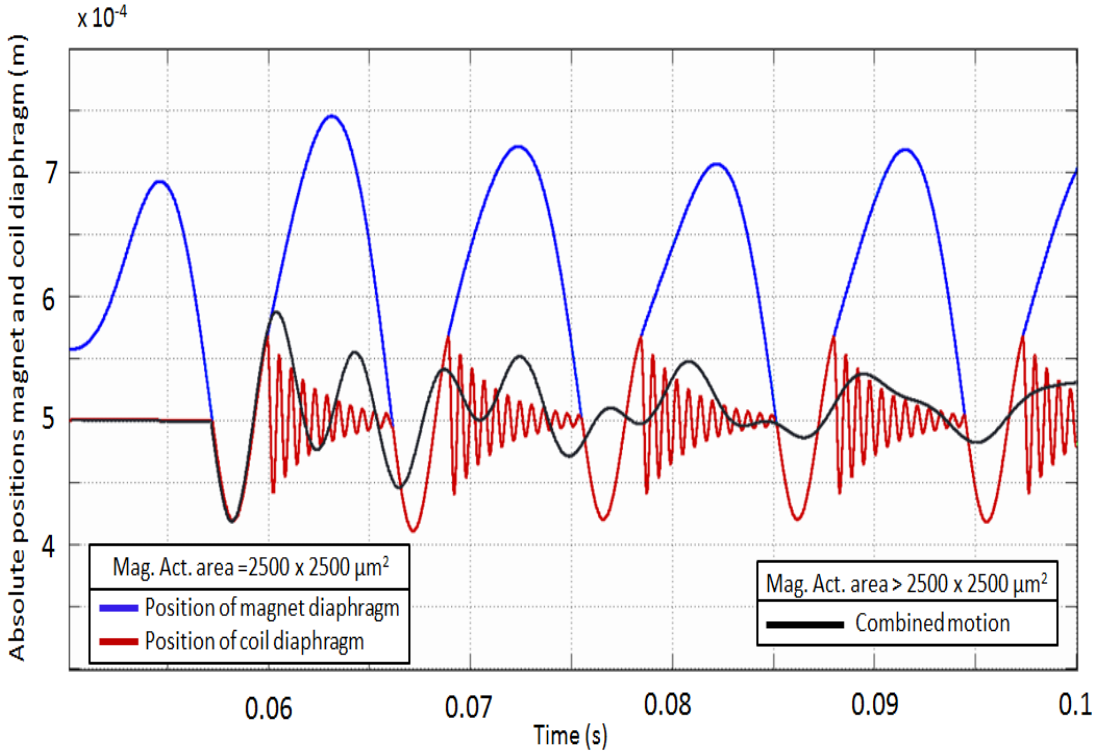

Figure 2.16. Effect of magnetic actuation area on realization of separate and combined motion of magnet and coil diaphragm.

As magnetic actuation area increases, the catch point (release height of the diaphragm) also increases, resulting high voltage and power levels (Figure 2.15). However, an increase in magnetic actuation causes the magnetic attraction force to be stronger than the tension force (2.24) all the time, resulting in a combined motion as presented in Figure 2.16.

Realization of the frequency up-conversion by sweeping the magnetic actuation area states that increasing the magnetic actuation directly affects the catch and release points of the coil diaphragm. The catch point of the coil diaphragm is the release height of the coil diaphragm which is the most important parameter for achieving higher voltage levels at the same size without increasing the device dimensions.

Table 2.1 shows the relation between the magnetic actuation area, release height of the coil diaphragm and accordingly induced voltage and power levels.

Table 2.1. Effect of varying magnetic actuation area on the performance of the generator.

Parameters	Magnetic actuation area			
	1000x1000 μm^2	1500x1500 μm^2	2000x2000 μm^2	2500x2500 μm^2
Release height (μm)	21	33	51	76
Resonance frequency of coil diaphragm (Hz)	1960	1883	1799	1702
Peak voltage (mV)	10	15,2	22,4	31,5
RMS voltage (mV)	3,52	5,3	8	11,1
Peak power (μW)	0,052	0,12	0,258	0,514
RMS power (μW)	0,0076	0,017	0,0396	0,0795

An increase in the magnetic actuation area, keeping all other parameters constant causes an insignificant decrease in the resonance frequency of the coil diaphragm, but an enormous increase in release height of the coil diaphragm (Figure 2.17). Accordingly, generated power levels increase in response to the increased release height of the coil diaphragm (Figure 2.18). This results in an improvement in generated power levels up to 0.5 μWatts.

Table 2.2 shows the improved parameters and simulation results for the generator. A sample simulation of the model using a MEMS chip size of 10 x 8.5 x 2.5 mm^3 is depicted in Figure 2.19. Simulations predict the expected maximum voltage and power from the second generation design as 15.2 mV and 119 nW, respectively.

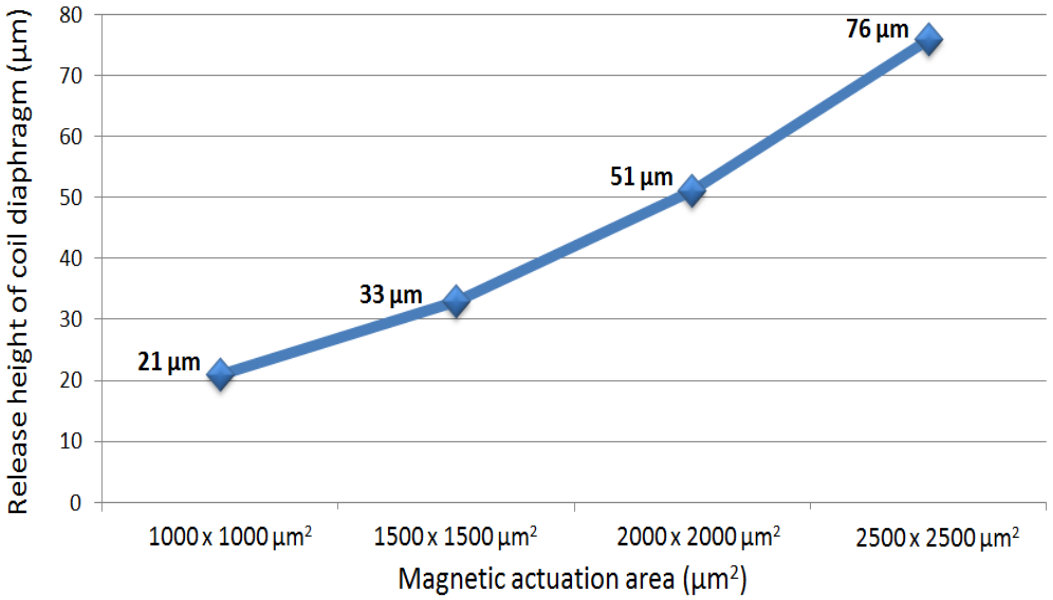

Figure 2.17. Effect of magnetic actuation area on release height of the coil diaphragm.

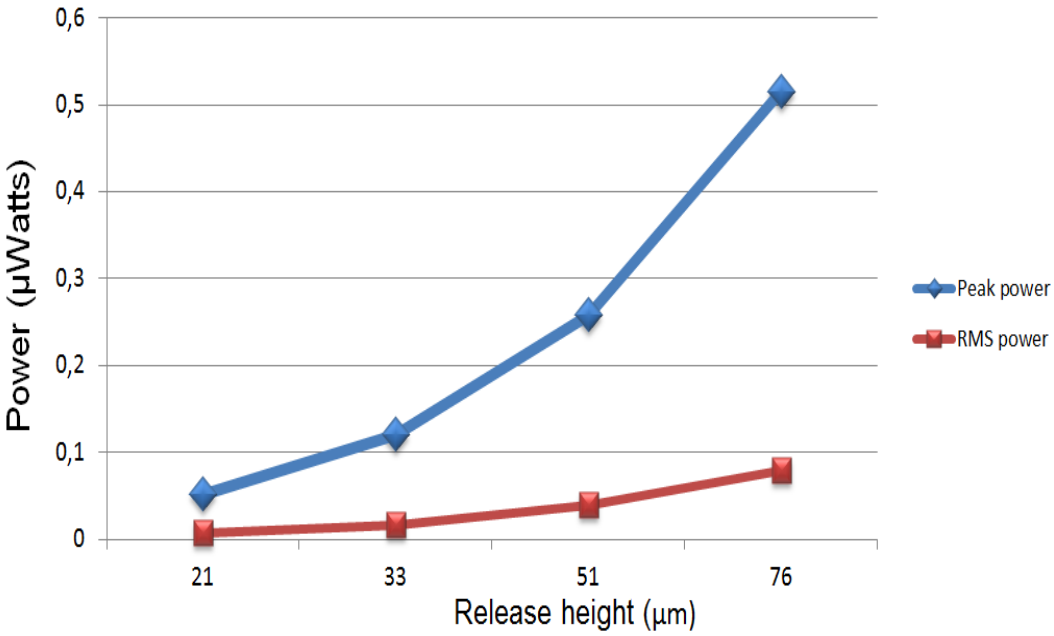

Figure 2.18. Generated power levels versus release height of the coil diaphragm.

Table 2.2. Simulation parameters of the generator.

Input vibration frequency	50-200 Hz
Magnet type	NdFeB (1.18 T)
Magnet dimensions	3.8 x 3.8 x 1.5 mm^3
Device dimensions	10 x 8.5 x 2.5 mm^3
Natural freq. of coil diaphragm	1.8 kHz
Coil diaphragm size	3800 x 3800 x 20 μm^3
Material for magnetic actuation	Nickel
Magnetic actuation area	1500 x 1500 x 9 μm^3
Diaphragms structural material	Parylene C
Length of each diaphragm arm	1000 μm
Width of each diaphragm arm	555 μm
Thickness of each diaphragm arm	20 μm
Total number of diaphragm arms	16
Magnet area on the diaphragm	3.95 x 3.95 mm^2
Natural freq. of magnet diaphragm	114 Hz
Release height of coil diaphragm	33 μm
Effective frequency range of the device	50-200 Hz
Distance between magnet and coil diaphragm	500 μm
Magnetic flux density	0.19 Tesla
Coil width	10 μm
Coil spacing	10 μm
Coil thickness	10 μm
Coil resistance	143 Ω
Number of coil turns	96
Peak voltage output	15.2 mV
RMS voltage output	5.8 mV
Peak power output	119 nW
RMS power output	21.1 nW

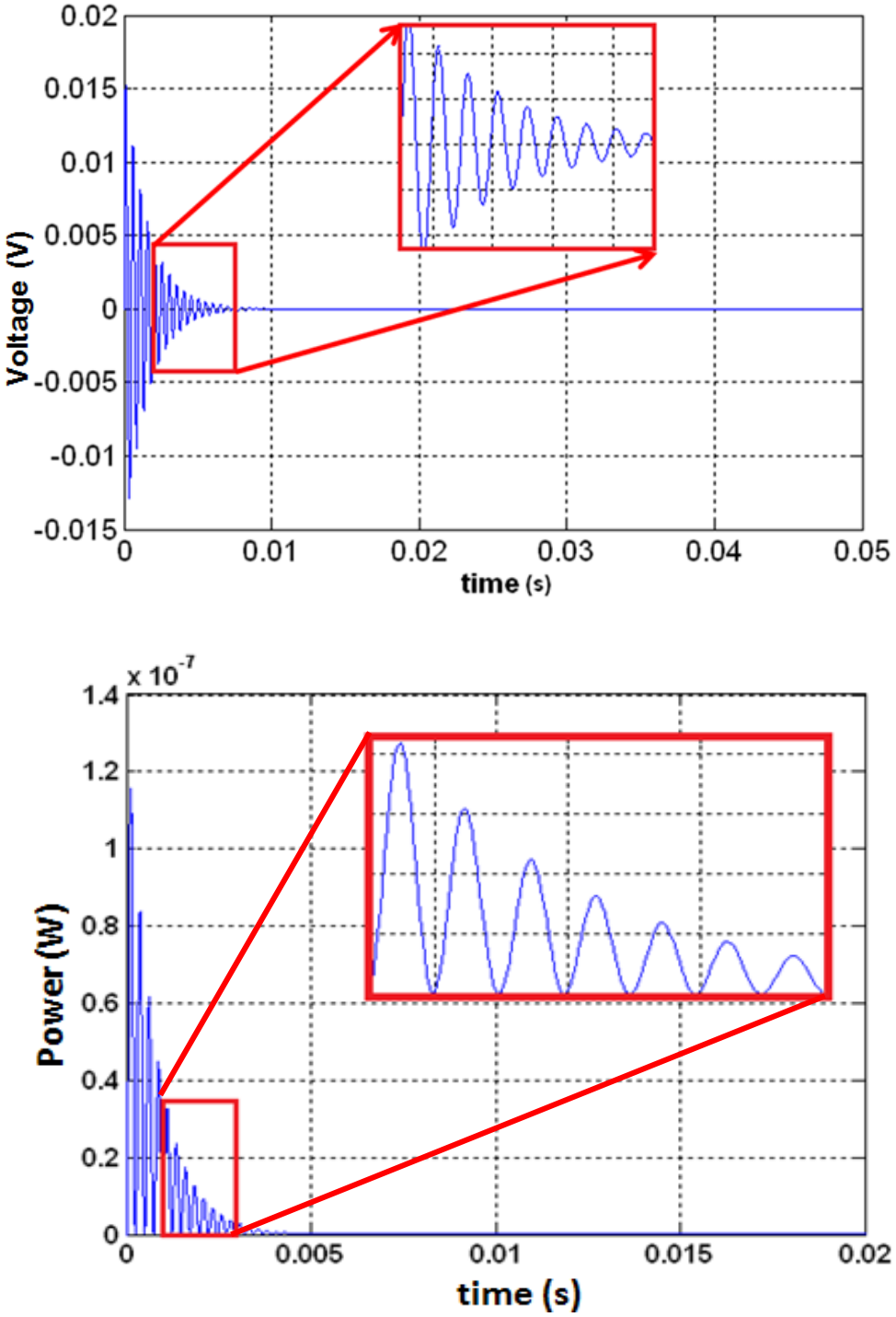

Figure 2.19. Simulation results for voltage output (top) and power output (bottom).

2.4 Conclusion

This chapter presented a micro generator design for harvesting energy from low frequency environmental vibrations within the scope of this thesis study. A detailed mathematical analysis and simulation parameters with governing motion equations have been given. These equations and parameters are then automated in a development tool engine in order to measure the performance of the generator with minimum incremental effort. The tool takes design and input parameters as input and estimates the mechanical parameters of the design, voltage and power output levels. These results are considered in fabrication steps especially for the mechanical design. With the proposed design, more than three orders of improvement is expected with respect to the previous one in term of generated power. Coil resistance is reduced to 143 Ω, synchronization and phase shift problem is eliminated. In the next chapter, the macro scale prototyping of the generator will be discussed.

CHAPTER 3

MACRO SCALE PROTOTYPING OF THE ENERGY HARVESTER

This chapter presents the design, fabrication and test results of the macro scale prototypes of the micro generator for verifying the feasibility of the frequency up-conversion with two diaphragms and for investigating the important parameters affecting the performance of the generator. In this scope, two different prototypes are fabricated: one having metal springs and the other one having rubber springs. First, Section 3.1 gives the properties of these macro scale prototypes. This is followed by the fabrication steps of the prototypes in Section 3.2. Afterwards, Section 3.3 presents the test setup. Finally, the chapter is completed with the presentation of the experimental results in Section 3.4.

3.1 Properties of the Macro Scale Prototype

Figure 3.1 depicts the schematic of the macro model for the proposed power generator consisting of two diaphragms, one carrying a magnet and the other carrying a coil and a magnetic piece. The diaphragms having different resonance frequencies are connected to a common frame and the magnetic frequency up-conversion is realized via the pull and release mechanism between the magnet and the magnetic piece.

3.1.1 Metal Spring Prototype

Figure 3.2 shows the fabricated metal spring energy harvester prototype. In this prototype, the diaphragms are connected to a fixed frame via metal springs. The upper diaphragm having lower resonance frequency carries a NdFeB magnet, and the lower diaphragm carries a hand wound coil and a magnetic piece. The feasibility of the prototype is verified by converting 6 Hz external vibrations up to 85 Hz, implementing 25 coil turns, resulting a maximum voltage and power levels of 11.1 mV and 5.1 μW, respectively (Figure 3.3).

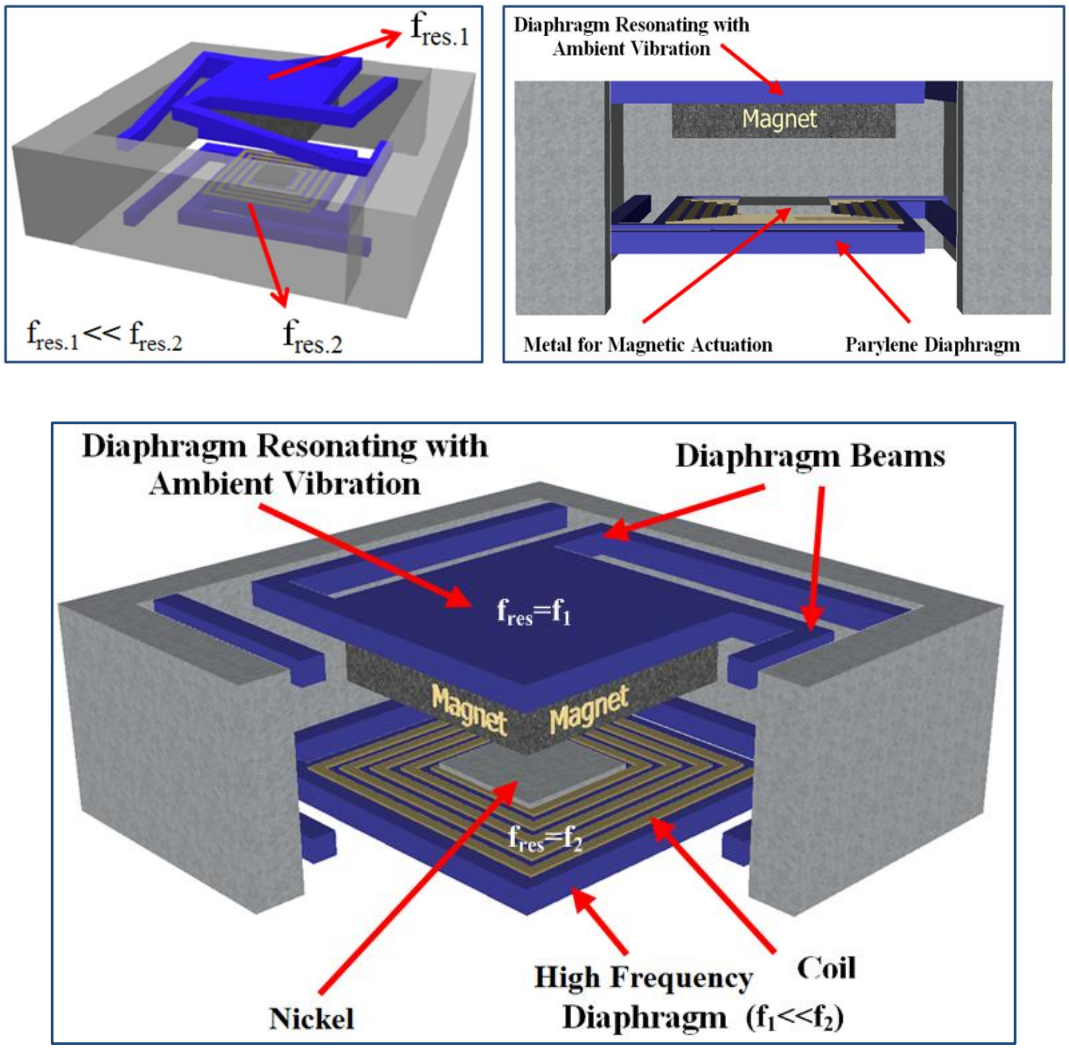

Figure 3.1. The proposed generator system.

Although the frequency up-conversion concept is realized by the test results, requirements of high acceleration levels caused the prototype to be tested with human motions by which high acceleration and displacement levels can be achieved with respect to vibration exciter. This aroused the need for the fabrication of another macro prototype in order to have test results by controllable input and excitation parameters with vibration exciter.

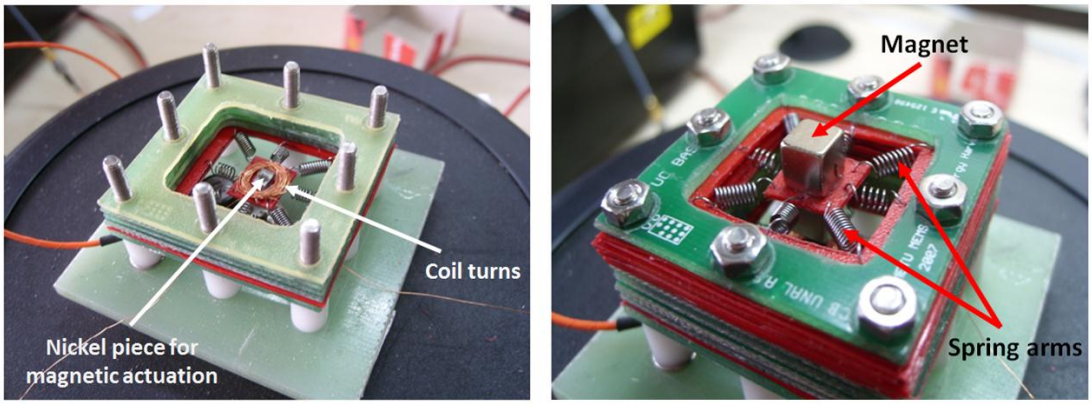

Figure 3.2. First macro scale prototype of the generator for proof of concept, coil diaphragm (left), the whole system (right).

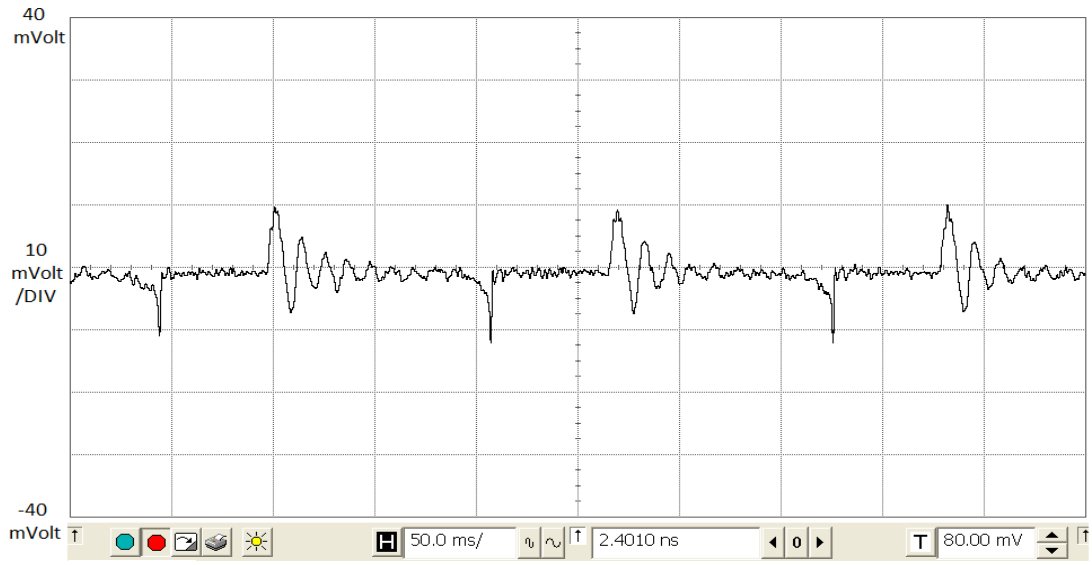

Figure 3.3. Voltage output from the macro prototype, realizing the frequency up-conversion.

3.1.2 Rubber Spring Prototype

The requirement of lower acceleration levels for accurate test results aroused the use of rubber springs instead of metal springs. Changing the metal springs with rubber springs also requires high precise alignment. The rubber springs need to be placed in such a way to realize the motion of the diaphragms along z direction. Accordingly, the alignment of the two diaphragms is important for the catch and release operation. The magnet and the magnetic piece need to move at the same direction for proper catch and release operation, realizing the frequency up-conversion. Therefore, the fabrication of the second macro prototype has been carried out in high precision automated CNC machines. The fabrication of the prototype is explained in the next section.

Introducing rubber springs in the macro model provides the prototype working at a tunable frequency range. Proper operation has been achieved at different external frequency ranges of 2-30 Hz with the help of rubber springs which makes the resonance frequency of each diaphragm tunable. The proposed power generator is able to fit in a wide range of energy harvesting applications covering low frequency vibrations and high frequency environments due to the adjustability of the rubber springs. The feasibility of the prototype for very low frequency and acceleration levels is also verified by operating the prototype at 2 Hz with a maximum peak acceleration of 0.024g which is in the range of vibrations such as ones arousing from human motions and building and tree vibrations [22].

The upper diaphragm carries a magnet while the lower one carries the pick-up coil and the magnetic piece for actuation. The upper diaphragm resonates with vibrations in the range of 2-30 Hz. On the other hand, the lower diaphragm has a higher natural resonance frequency range of 20-200 Hz. The exact resonance frequency values of the diaphragms are set by adjusting their rubber springs. When the upper diaphragm starts resonating with external vibrations, the magnet pulls and releases the magnetic piece, making the lower diaphragm resonate at its resonance frequency, realizing the magnetic frequency up-conversion. Power is generated through electromagnetic

induction, with relative position change of the magnet and the coil. Both of the diaphragms are fixed to a common frame via rubber springs.

As stated before, the prototype is composed of two frames which are combined with screws at the end of the fabrication. While the whole prototype can be seen in Figure 3.4, the lower diaphragm which has the coil turns and magnetic piece for frequency up-conversion is given in Figure 3.5.

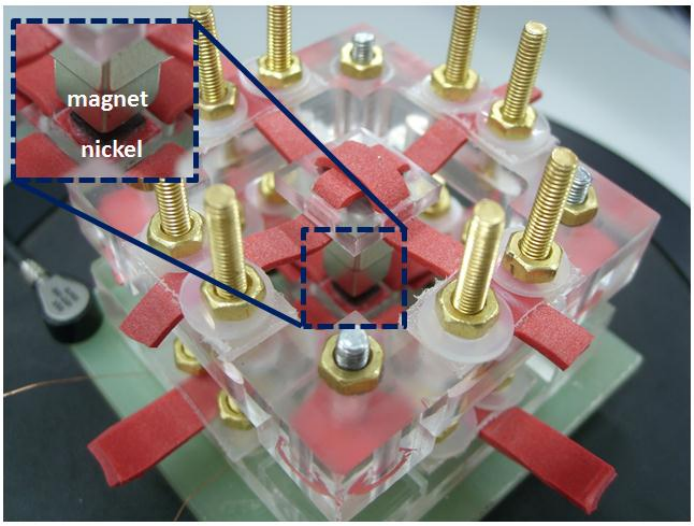

Figure 3.4. Second macro scale prototype of the generator.

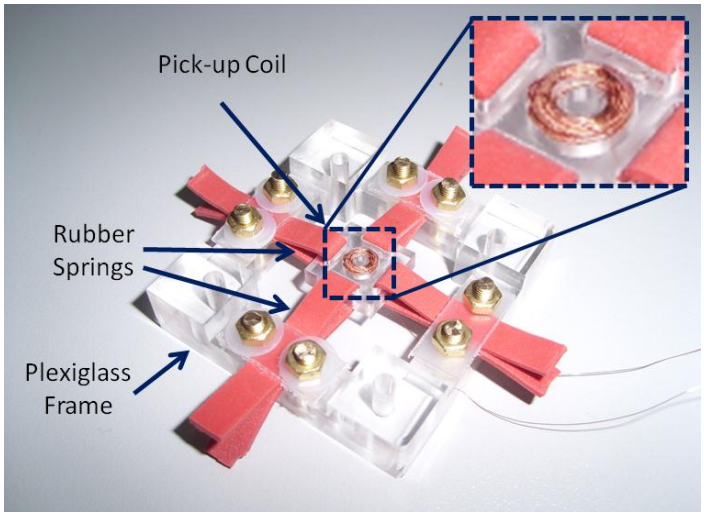

Figure 3.5. High frequency coil diaphragm of the generator.

3.2 Fabrication of the Macro Prototype

The fabrication of the macro prototype has been carried out in a highly automated flexible manufacturing laboratory in Çankaya University. The manufacturing system consists of two CNC machines of high level technology and a five axis robot. One of the CNC machines, the milling machine is the part of the machining center, while the other machine, turning machine is the element of turning center. Each machine is connected to computers over the control boxes. The fabrication in CNC milling machine is controlled by the software via the controller boxes. This software has a nc (numerical control) code development interface, realizing the fabrication of the milling parts by nc codes.

The macro prototype has been fabricated as two different frames, to be combined at the end of the fabrication. The frames are fabricated in such a way that the space between the two frames will be enough for the magnet movement and coil diaphragm displacement. Frames are fabricated from a plexiglass material which is suitable for the machining operation in CNC milling machine. Plexiglass is a transparent material which makes assembly and testing operations visible at the same time (Figure 3.6).

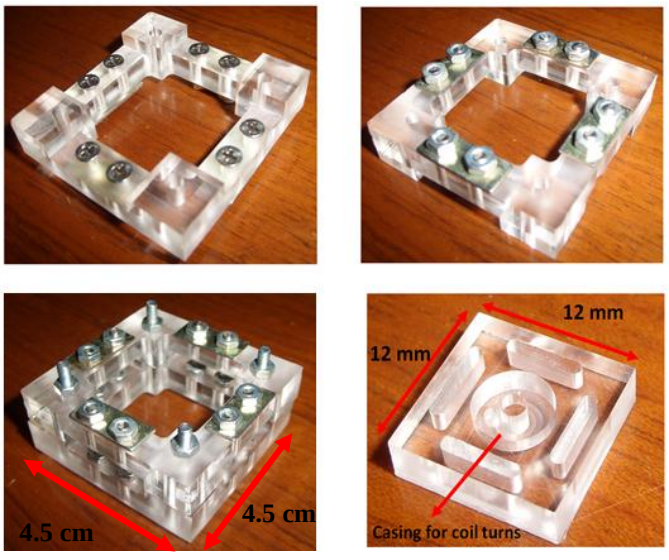

Figure 3.6. Fabricated frames for magnet diaphragm and coil diaphragm (top), assembly of the frames and casing for the coil turns (bottom).

3.3 Test Setup

The fabricated rubber spring macro prototype is tested by using a vibration shaker system. Figure 3.7 shows the test setup and related equipment. Test setup is composed of a shaker table, a control unit, an amplifier, accelerometer and software interface. The user interface provides the user to enter the desired input and test parameters by a user interface program which is a part of the test setup. Tests can be carried out in a frequency range of 2 Hz to 20 kHz and up to an acceleration of 75 g.

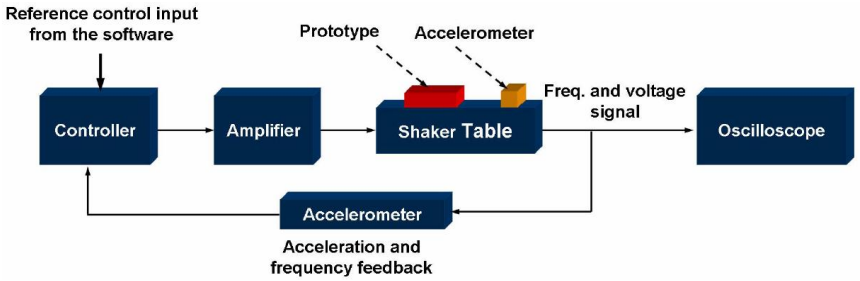

Figure 3.7. Block diagram of the test setup.

3.4 Experimental Results of the Prototype

Proposed micro power generator structure has been tested and feasibility of the frequency up-conversion has been verified and also tunability of the resonance frequency is experimentally verified by operating the same device at 2 Hz, 13 Hz, and 30 Hz external vibrations via adjusting the rubber springs for the desired resonance frequency. Table 3.1 gives a summary of the different prototype configurations and the corresponding test results. Figure 3.8 (a) and (b) present the output voltage waveform of the two sample generator configurations operating at 2 Hz and 13 Hz, respectively.

For a 2 Hz, 3 mm peak-to-peak external vibration condition, corresponding to a very low rms acceleration value of 0.017g, the prototype proved to generate 0.34 mV rms voltage and 13.7 nW rms power, with an up-converted resonance frequency of 23 Hz. When the vibration conditions are set as 13 Hz frequency and 7.5 mm peak-to-

peak displacement, the generated output voltage and power reaches to 5.2 mV and 3.21 μW, with the lower diaphragm resonance frequency adjusted as 200 Hz. It should also be noted that the adjustment of the distance between the two diaphragms is also necessary as well as adjusting their resonance frequencies for proper operation of the power generator.

Table 3.1. Specifications and performance parameters of the tested prototype.

Excitation frequency	**2 Hz**	**13 Hz**	**30 Hz**		
Magnet type	NdFeB (1.18 T)				
Magnet dimensions	8x8x16mm^3		8x8x24mm^3		
Magnetic piece material	Nickel		NdFeB (1.18 T)		
Magnetic piece dimensions	2.5x2.5x0.5 mm^3		2.5x2.5x2.5 mm^3		
Distance btw. magnet and coil turn	2 mm	5 mm	8.5 mm		
Catch distance between two diaphragms	0.5 mm		4 mm		
Number of coil turns	50		50	100	250
Coil resistance	2.1 Ω		2.3 Ω	3.3 Ω	7.9 Ω
Coil wire diameter	120 μm				
Coil inner diameter	2 mm		3.3 mm		
Coil outer diameter	4 mm		4.5mm	5.4mm	9.5mm
Device dimensions	32x32x22mm^3				
Upper diaphragm f_{res} (f_1)	2 Hz	13 Hz	30 Hz		
Lower diaphragm f_{res} (f_2)	23 Hz	200 Hz	90 Hz		
Input displacement	3 mm	7.5 mm	7.3 mm		
Input peak acceleration	0.024 g	2.54 g	13.2 g		
Input RMS acceleration	0.017 g	1.78 g	9.34 g		
Peak output voltage	2 mV	34.5 mV	13 mV	37 mV	104 mV
Peak output power*	476 nW	141.6 μW	18.3 μW	104 μW	342 μW
RMS output voltage	0.34 mV	5.2 mV	3.2 mV	6.8 mV	29 mV
RMS output power*	13.7 nW	3.21 μW	1.1 μW	3.5 μW	26.6 μW

* For an equivalent resistive load.

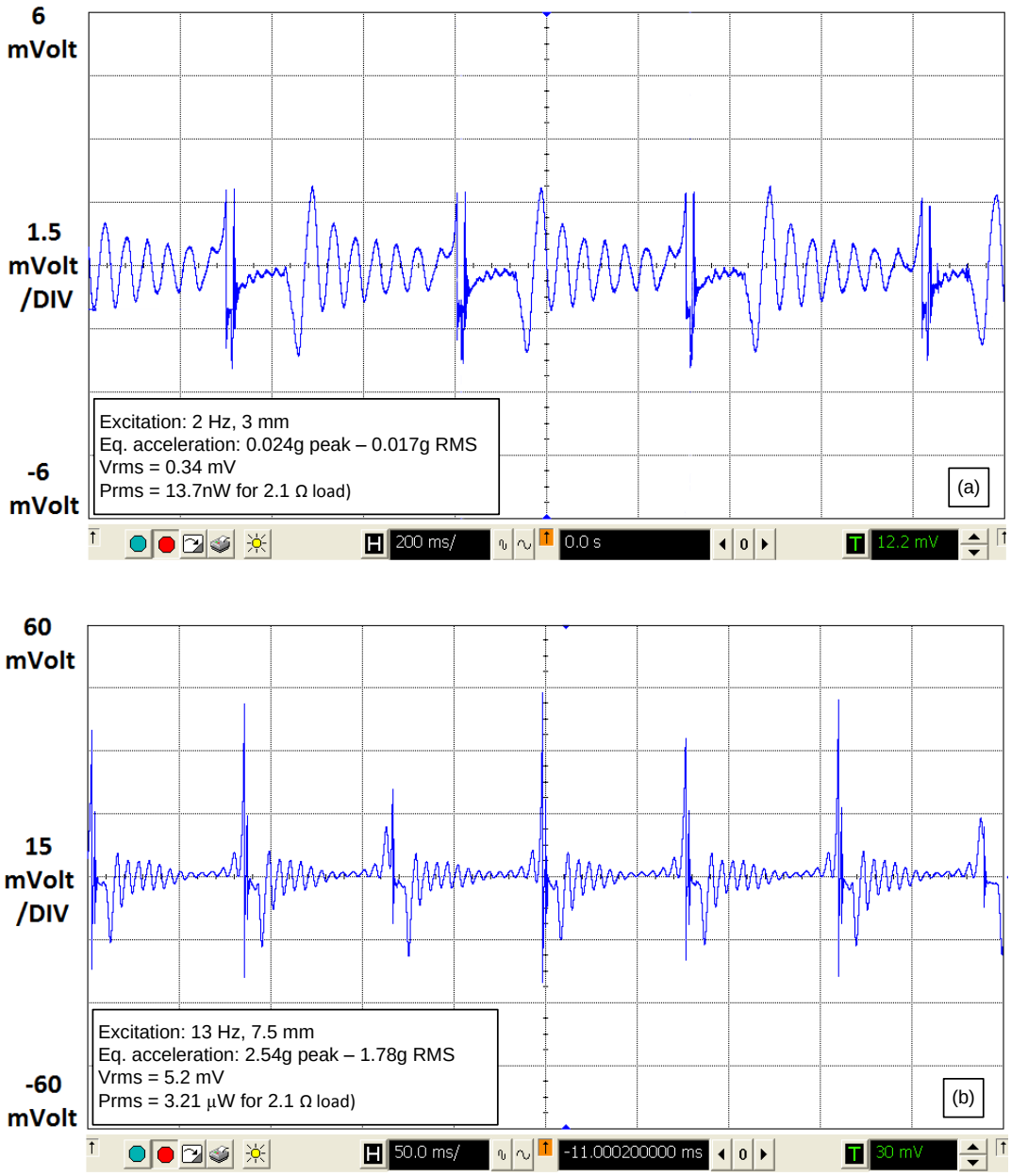

Figure 3.8. Measured voltage output of the energy harvester in response to vibrations of (a) 2 Hz and (b) 13 Hz.

Figure 3.9 shows the generated voltage and power levels from the prototype for different resonance frequency and coil turn values. The highest rms power level of 26.6 µW is obtained for a configuration where 9.34g rms vibrations at 30 Hz are up converted to 90 Hz, and a 250-turn coil is used.

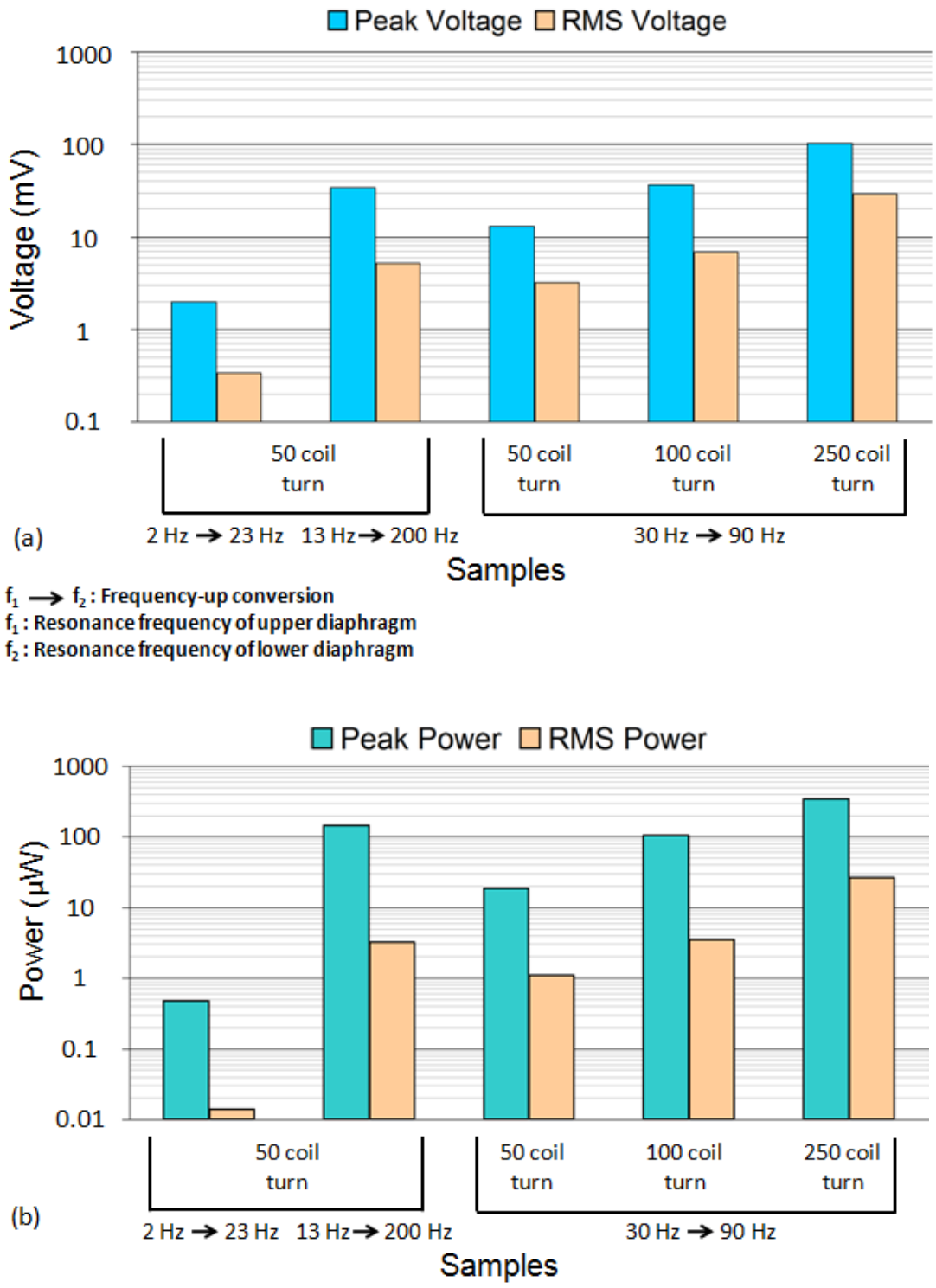

Figure 3.9. Measured voltage (a) and power (b) output at 2 Hz, 13 Hz, and 30 Hz with varying number of coil turns.

3.5 Conclusion

This chapter presented the macro prototypes of the proposed micro generator. Two different prototypes are fabricated: one having metal springs and the other one having rubber springs. In metal spring prototype, the diaphragms are connected to a fixed frame via metal springs. The upper diaphragm having lower resonance frequency carries a NdFeB magnet, and the lower diaphragm carries a hand wound coil and a magnetic piece. The feasibility of the prototype is verified by converting 6 Hz external vibrations up to 85 Hz. Although the frequency up-conversion concept is realized by the test results, requirements of high acceleration levels caused the prototype to be tested with human motions by which high acceleration and displacement levels can be achieved with respect to vibration exciter. This aroused the need for the fabrication of another macro prototype in order to have test results by controllable input and excitation parameters with vibration exciter.

The requirement of lower acceleration levels for accurate test results aroused the use of rubber springs instead of metal springs. Introducing rubber springs in the macro model provides the prototype working at a tunable frequency range. Proper operation has been achieved at different external frequency ranges of 2-30 Hz with the help of rubber springs which makes the resonance frequency of each diaphragm tunable. The feasibility of the prototype for very low frequency and acceleration levels is verified by operating the prototype at 2 Hz with a maximum peak acceleration of 0.024g resulting in 2 mV and 476 nW power level.

As a result, experimental results verify the feasibility of the new architecture. In the next chapter, the fabrication of the micro generator will be discussed.

CHAPTER 4

THE FABRICATION OF MICRO GENERATOR

This chapter explains the micro fabrication steps of the micro generator. Layout drawings of the masks are drawn by Tanner Tools® Layout editor®. As stated before, the new topology consists of an upper and a lower diaphragm, one holding the coil turns and other diaphragm stands for magnet assembly (Figure 4.1). Firstly, Section 4.1 explains the properties of the new topology and Section 4.2 gives the schematic drawing of the wafer. Afterwards, Section 4.3 explains the microfabrication steps of the generator. This chapter is finalized with the photos of the fabrication steps.

4.1 General View of the Micro Generator

Micro generator consists of an upper and a lower diaphragm (Figure 4.1). Both of the diaphragms are fabricated from several Parylene C layers to achieve a thickness of 20 μm. The lower diaphragm (coil diaphragm) has 96 coil turns with 10 μm width and 10 μm thick metal layers. Spacing between these metal layers is designed as 10 μm. For achieving higher voltage levels, two layers of coil turns are also deposited on the coil diaphragm which is shown on the wafer layout in Figure 4.2. Additionally, at the middle of the diaphragm a 1500 x 1500 x 9 μm^3 metal layer (nickel) is formed for magnetic actuation. Other critical dimensions of the generator are given in layout drawing in Figure 4.1.

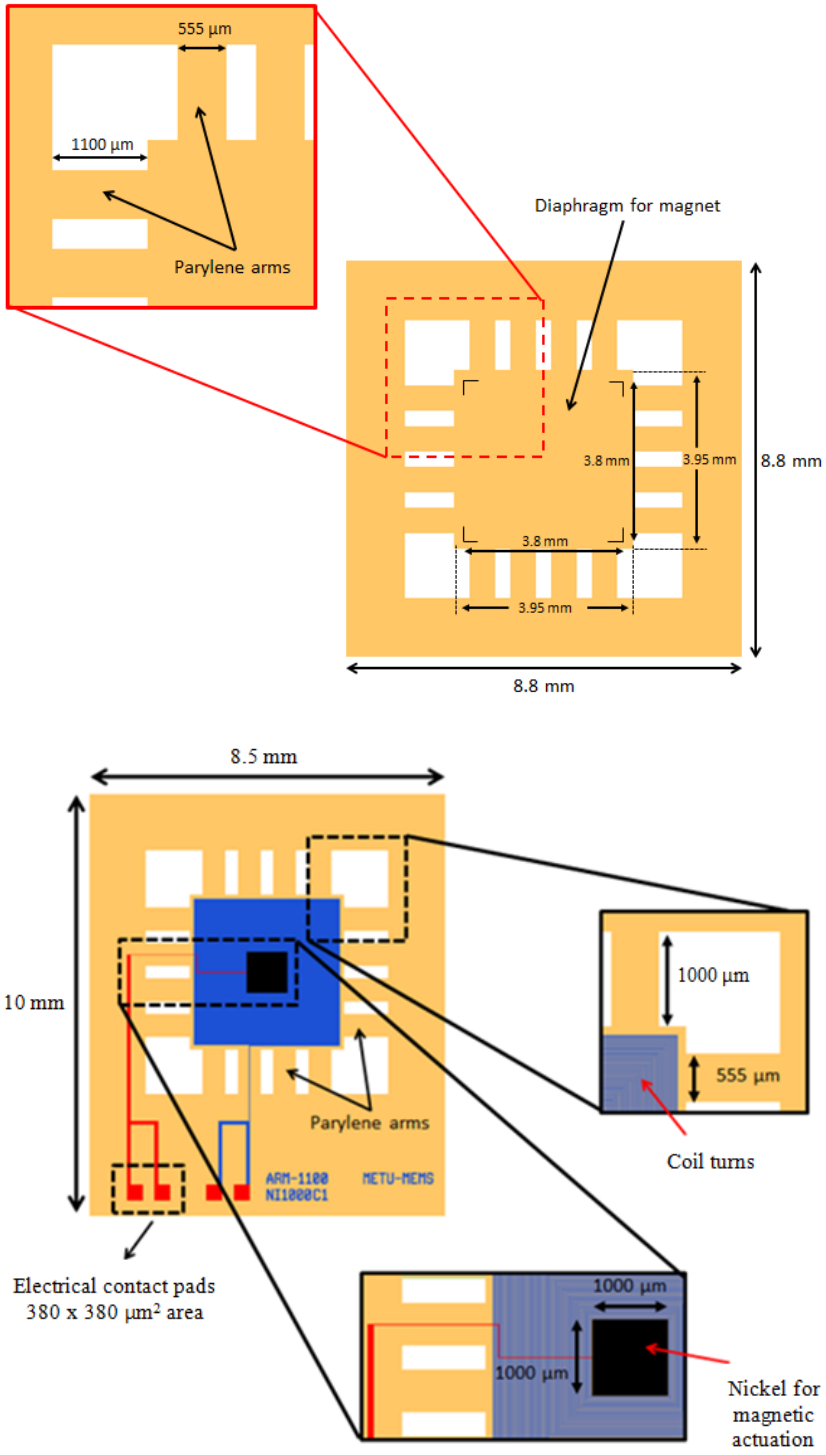

Figure 4.1. Schematic drawing of the frequency up-conversion design, magnet diaphragm (top), coil diaphragm (bottom).

4.2 Layout of the Whole Wafer

Figure 4.2 shows the layout of the wafer and the devices on this 4-inch wafer. Magnet diaphragm and coil diaphragm are both fabricated on the same wafer.

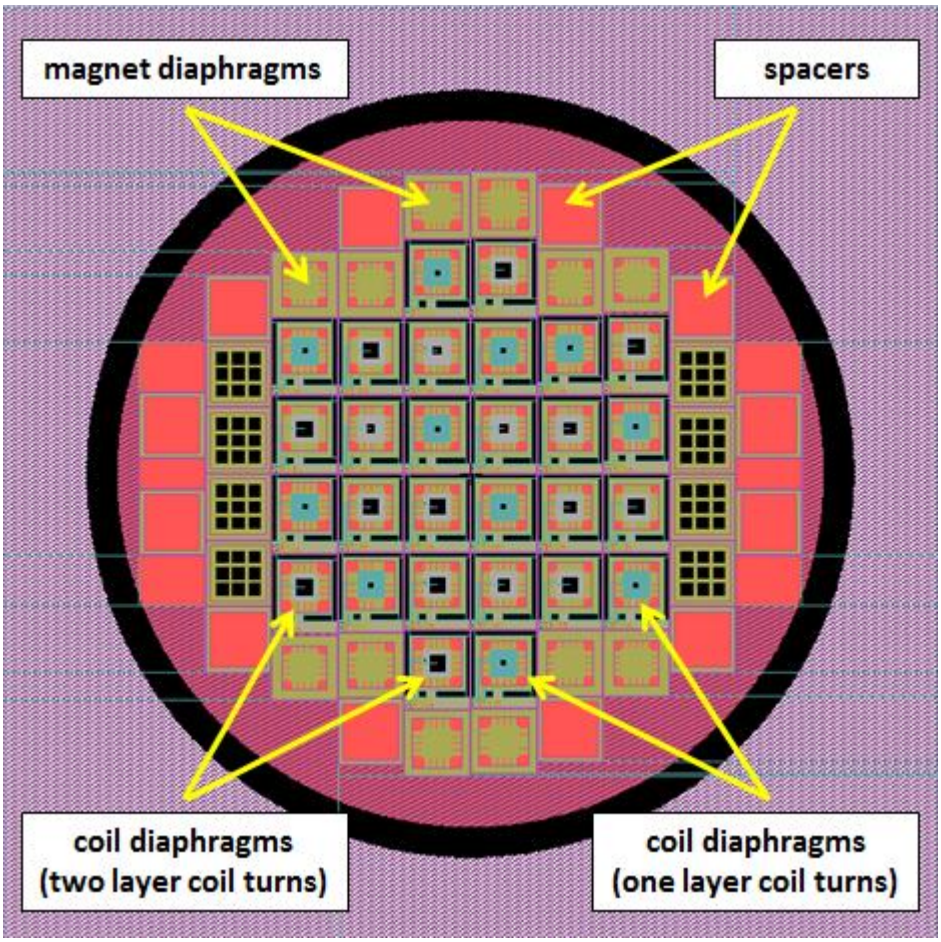

Figure 4.2. Layout of the 4-inch silicon wafer.

4.3 Fabrication steps of the Micro Generator

This section explains the fabrication steps of the designed micro generator. The micro generator is fabricated as two separate chips to be combined at the end of the process. These chips are fabricated on the same wafer that requires 8 masks which are designed and fabricated at METU-MEMS Center. The fabrication sequence is shown in Figure 4.3. A more detailed process flow is given in Appendix A.

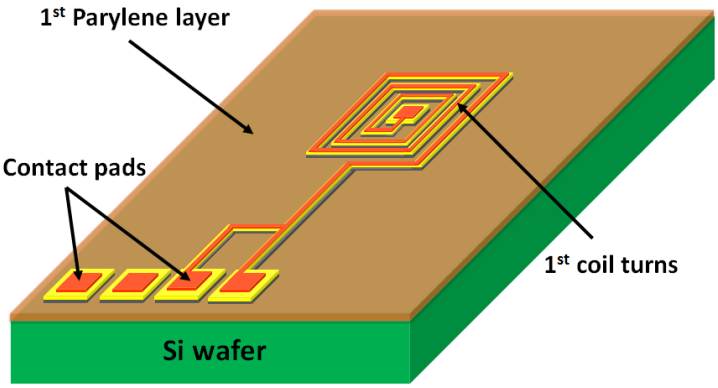

1st Parylene deposition + 1st coil turns by Au/Ti sputter and Cu electroplating.

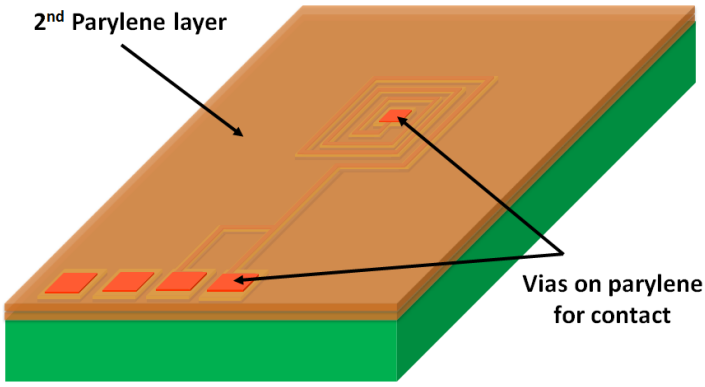

2nd Parylene deposition + via opening on parylene layers to get contact.

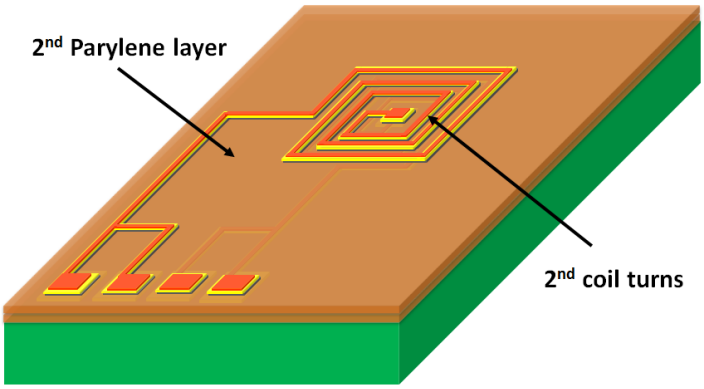

2nd Parylene deposition + 2nd coil turns by Au/Ti sputter and Cu electroplating.

Figure 4.3. The fabrication sequence of the micro energy harvester.

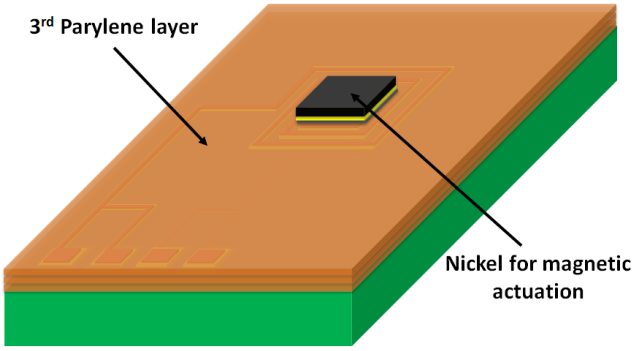

3rd Parylene deposition + nickel electroplating for magnetic actuation area.

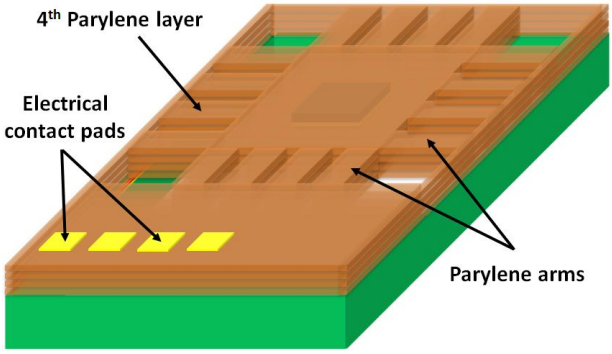

4th Parylene deposition + RIE for patterning diaphragm and DRIE for release.

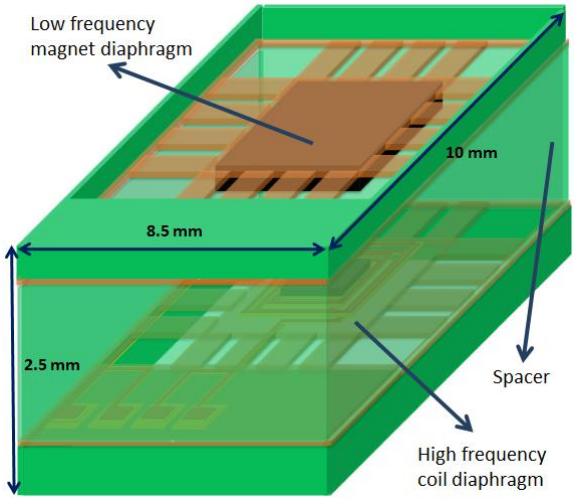

Assembly of the coil diaphragm and magnet diaphragm.

Figure 4.3. (cont'd).

At the end of the fabrication, fabricated chips on the wafer should be separated from each other. In order to eliminate the dicing step, the masks are drawn so that devices can be separated from each other by manually applying a light force between the devices on the wafer. All devices are attached to each other by a 200 μm length and 20 μm thick parylene layer. At the end of the fabrication, after the devices are released, they can be separated from each other by applying a light force on these parylene structures.

Masks and details of related processes are summarized in Table 4.1. The tolerance of the masks is set as 10 μm which is enough for the minimum feature size. The field types of each mask are also specified whether they are dark field or clear field.

Table 4.1. List of the masks used in micro fabrication of the micro generator.

Mask #	**Mask Name**	**Field type**	**Patterned or etched material**	**Description**
1	Ti-Au Sputtering before copper electroplating	Clear	Ti/Au	Form the first metal routes
2	Copper Electroplating	Dark	Cu	Form the first coil turns on first metal routes
3	Vias on parylene	Dark	Parylene	Etch parylene to form vias
4	Ti-Au Sputtering before copper electroplating	Clear	Ti/Au	Form the second metal routes
5	Copper Electroplating	Dark	Cu	Form the second coil turns on second metal routes
6	Nickel Electroplating	Dark	Ni	Form magnetic actuation area
7	Parylene	Clear	Parylene	Form the diaphragms
8	DRIE for Silicon	Dark	Silicon	Etch Si wafer from backside to release the devices

After giving a brief outline of the fabrication process, the detailed process flow of each step is explained in the following paragraphs. Figure 4.4 gives the process flow of the micro generator.

First, an oxide layer is formed on the backside of the silicon substrates. Next, a 5 μm-thick parylene is deposited to the front side of the wafer (a). Then, Ti/Au seed layer is deposited and patterned to form the coil turns. Copper is electroplated on the coil turns for increasing the thickness (b). As the next step, a second 5 μm thick parylene layer is formed on the electroplated copper to provide electrical isolation between the first and second metal layers and patterned at the contact areas in order to form via openings (c). Then, second seed layer is deposited and patterned and copper layer is electroplated to complete the metal routes (d). After forming the second metal, another parylene layer is deposited to increase the thickness and adjust the resonant frequency of the coil diaphragm (e). A 3rd seed layer is deposited, over it, a 9 μm thick nickel is electroplated to form the magnetic actuation area (f). A final layer of parylene is deposited to act as a protection layer for the magnetic actuation area and patterned to obtain the pad openings for external contacts (g). Next, by etching the sacrificial oxide, and DRIE step, devices are released and two separate set of chips are obtained (h). Magnet is placed on top of the parylene diaphragm (i). Finally, two chips are combined with a separator (j), finalizing the assembly of the energy harvester. Detailed fabrication process flow is also given in Appendix B.

The fabrication steps of the generator are summarized by photos of the wafer below considering the process flow. Figure 4.5 shows the coil diaphragm structure which has coil turns and contacts fabricated on the wafer. Figure 4.6 shows the electroplated nickel on the coil diaphragm for the interaction with the magnet. As the next step, after the electroplating step of nickel, the seed layer which is composed of Au/Ti needs to be removed. However, Au etchant attacks the electroplated nickel as shown in Figure 4.7. One of the solution approaches is the use of selective etchant for this process. Au selective etchant can be used as an alternative etchant to remove Au without attacking to nickel. Another solution method is the application of image reversal process in order to pattern the seed layer first before the electroplating step of nickel. Thus, etchant attack problem can be eliminated.

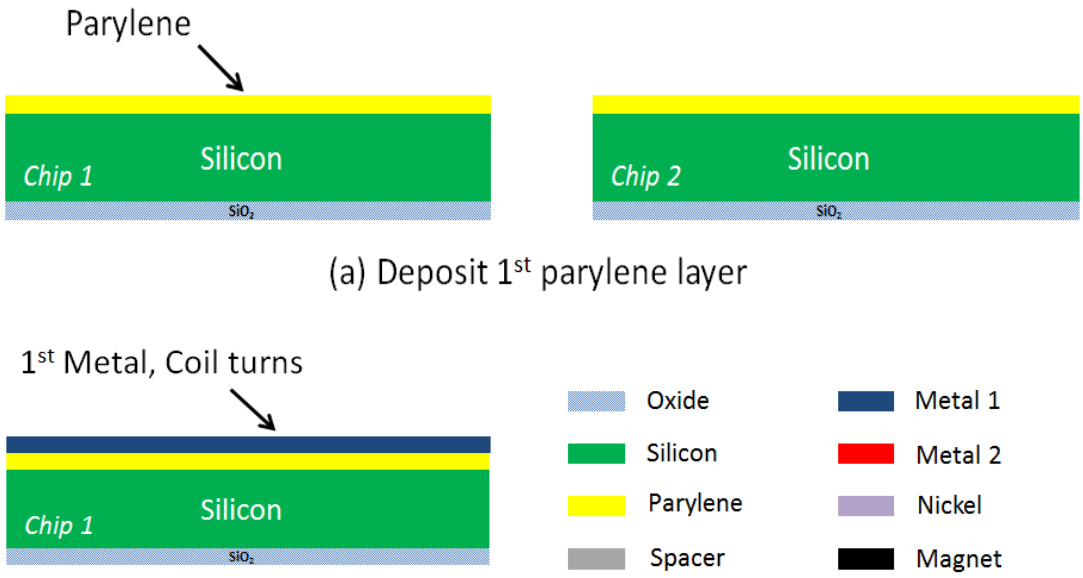

Figure 4.4. Micro fabrication steps of the generator.

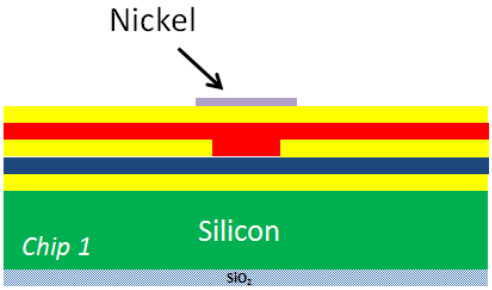

(f) Electroplating nickel for magnetic actuation

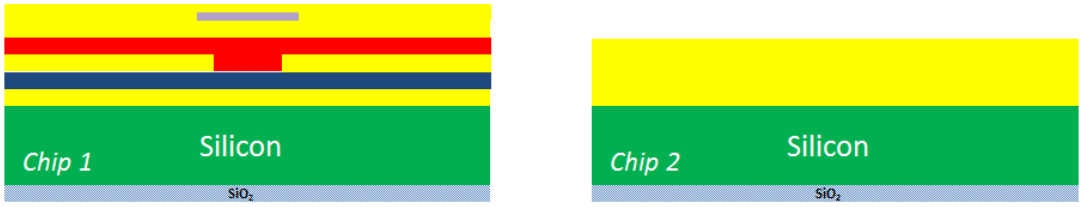

(g) Deposit and pattern final parylene layer

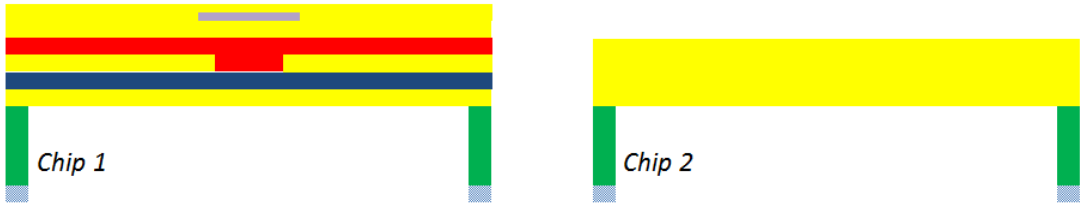

(h) Oxide etch and DRIE from backside to release the device

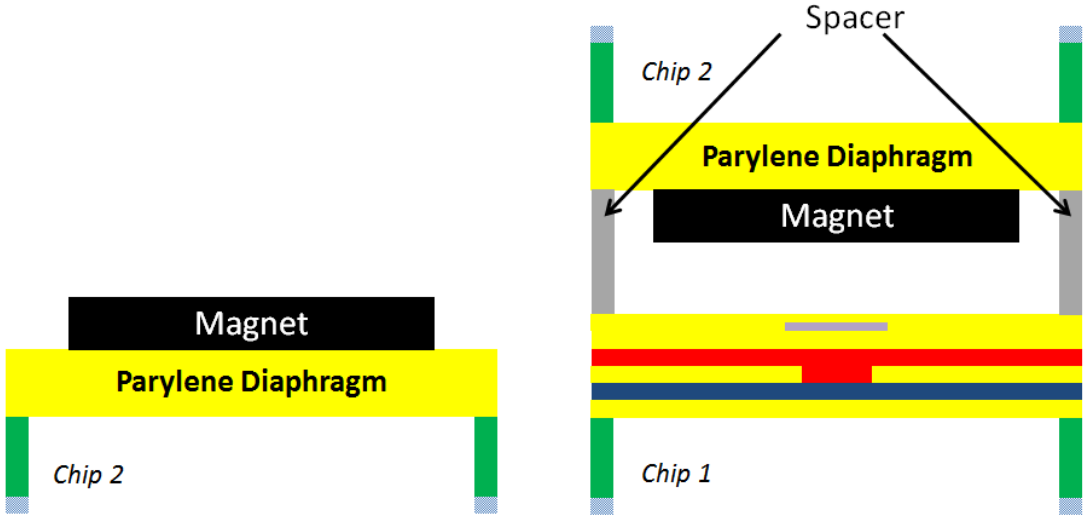

(i) Locating the magnet (j) Combining the two chips

Figure 4.4. (cont'd).

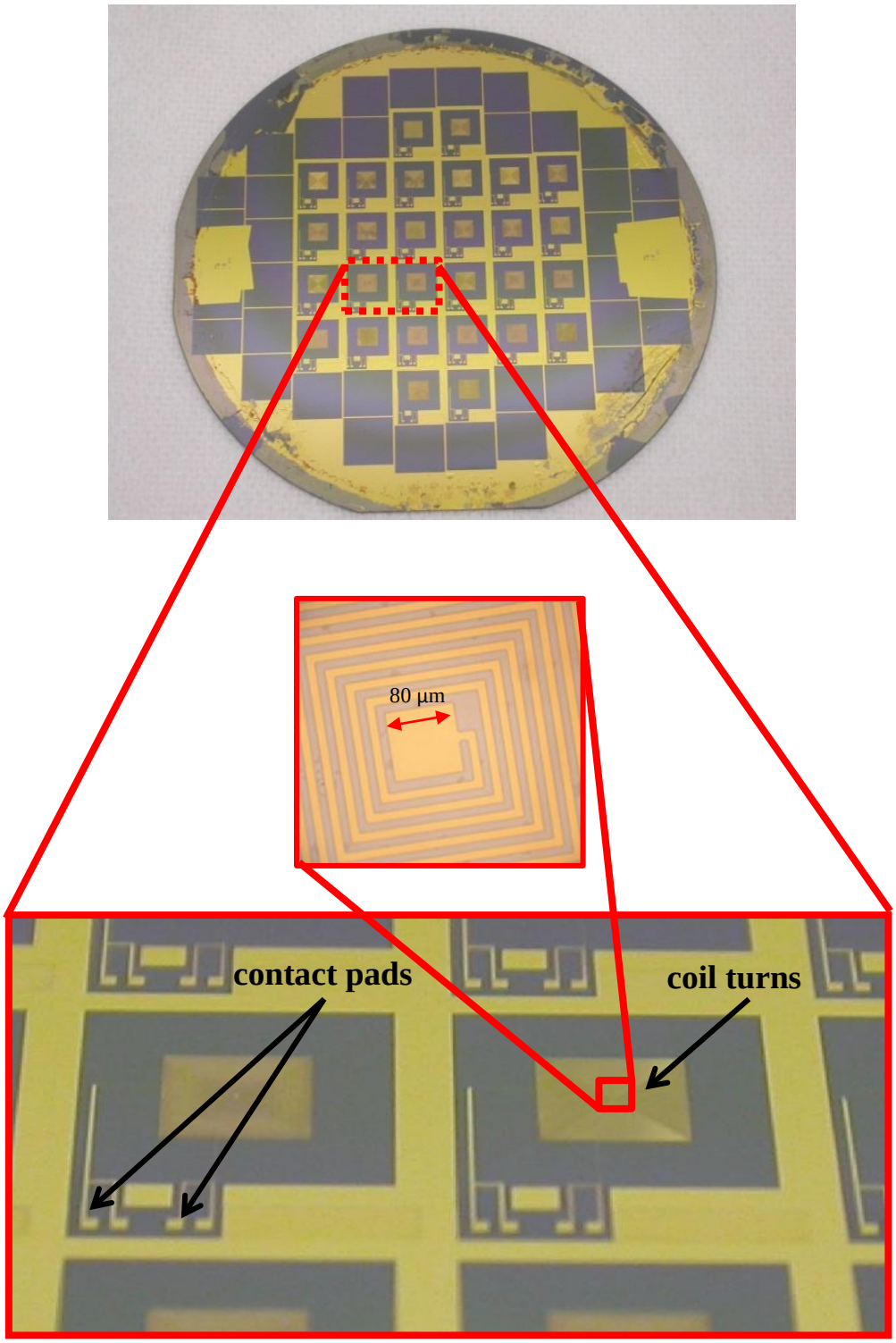

Figure 4.5. Fabricated coil turns and contact pads on coil diaphragm on a 4'' wafer.

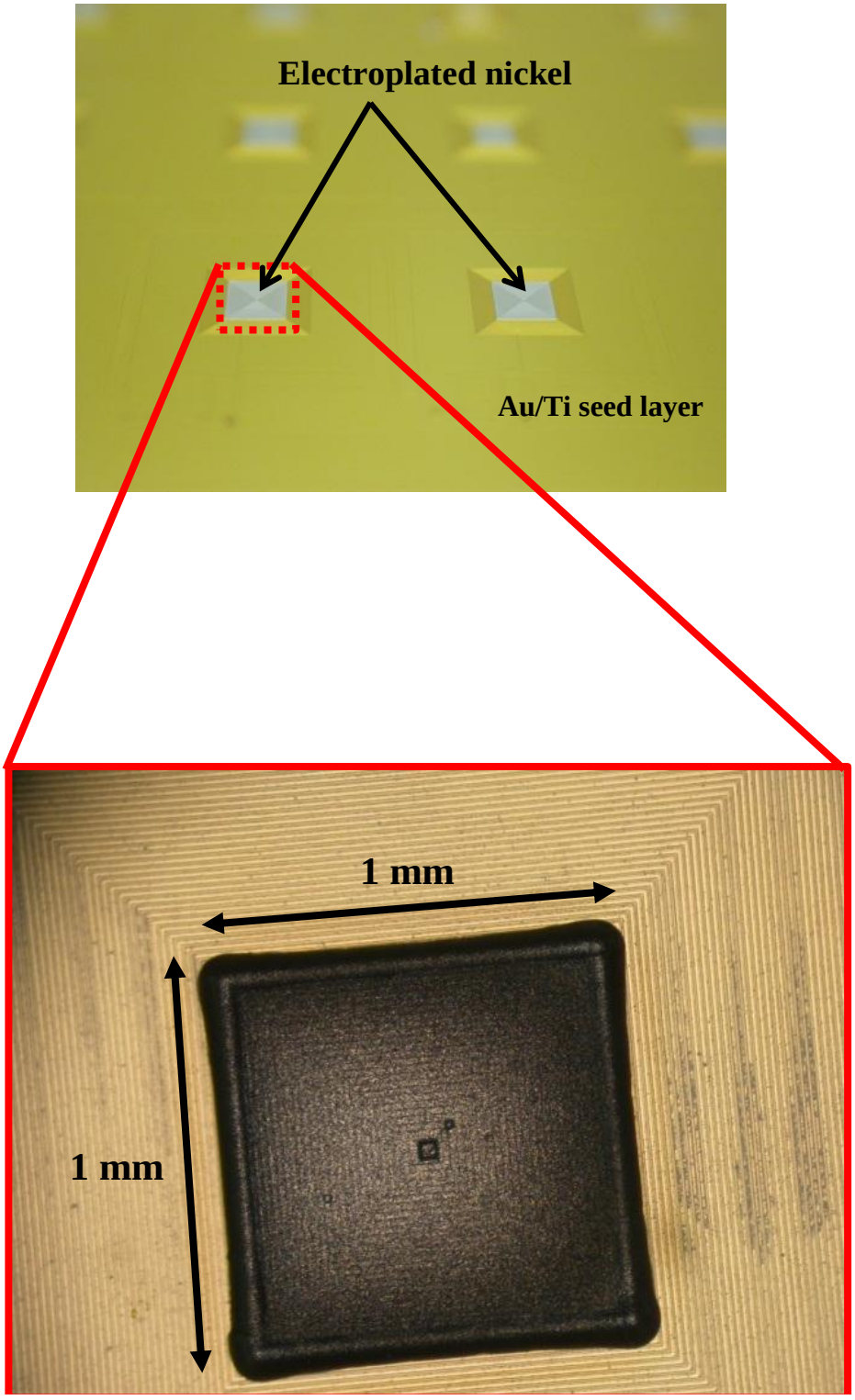

Figure 4.6. Electroplated nickel for magnetic actuation area.

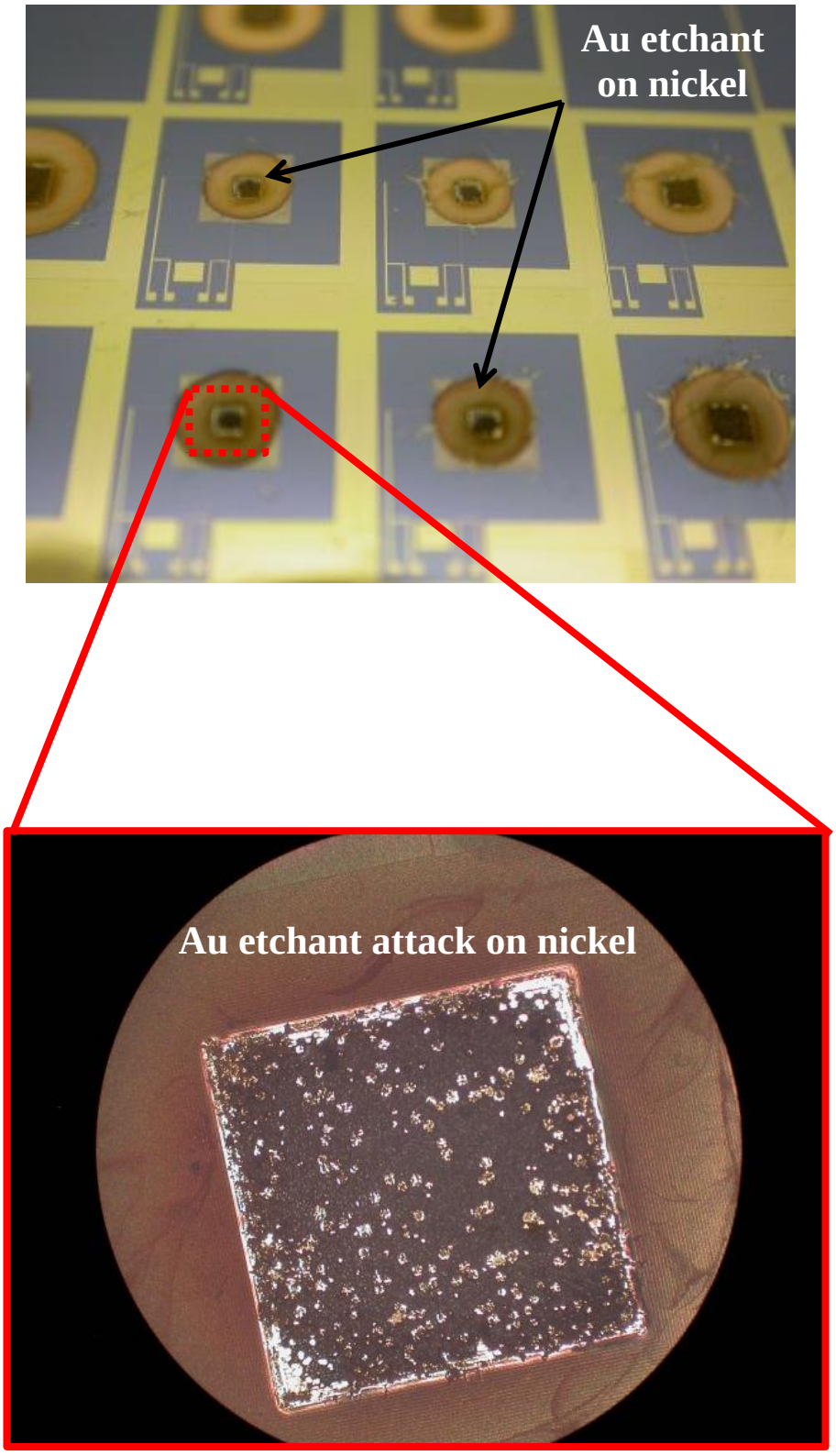

Figure 4.7. Au etchant attack on electroplated nickel.

4.4 Conclusion

This chapter presented the micro fabrication steps of the proposed generator. The properties of the proposed frequency up-conversion micro generator have been presented. Afterwards, fabrication steps including process flow are also given in detail.

The problems related with microfabrication have been discussed and solution approaches have been presented. Following the problems in microfabrication, fabrication photos are given in Figures 4.5, 4.6, and 4.7. Due to these problems, the fabrication of the devices could not be finalized, although almost all the fabrication steps have been concluded.

CHAPTER 5

CONCLUSIONS AND FUTURE WORK

This thesis study presented the design of a new electromagnetic type low frequency micro energy harvester structure utilizing the frequency up-conversion mechanism, fabrication, and characterization of two macro prototypes. Furthermore, a process flow has been designed for the fabrication of the structures with microfabrication techniques.

Within the scope of this study, the cantilever based frequency up-conversion design that has been previously developed in METU-MEMS Center has been improved in term of performance parameters, realizing the frequency up-conversion with a monolithic diaphragm instead of consecutive cantilevers. The main advantage of the proposed design is the use of a monolithic diaphragm instead of cantilevers, increasing the available area for coil turns, resulting in a higher voltage and power output levels. Also, integrating 20 consecutive cantilevers into the first generation module has not yielded in proportionate scaling of the output power compared to a single cantilever. This was due to the synchronization and resulting phase shift problem of the cantilevers as well as the mismatches in the resonance frequency of each cantilever, reducing the available aggregate power.

For predicting the performance of the proposed design in response to different design parameters, a user interface based development tool has been built up in Visual® Basic® environment. The tool includes the automation of the physical equations and additional modeling capabilities to achieve simulation accuracy for the generator performance.

In order to show the feasibility of the proposed structure, two macro prototypes of the micro generator have been fabricated and tested for performance measurements. The first prototype converts 6 Hz external vibrations up to 85 Hz by using metal springs. However, requirements of high acceleration levels caused the prototype to be tested with human movements by which high acceleration and displacement levels can be achieved with respect to vibration exciter. This aroused the need for the fabrication of another macro prototype in order to have test results by controllable input and excitation parameters with vibration exciter. Therefore, in the 2nd prototype, metal springs have been changed with rubber springs. The results show that at an excitation frequency of 30 Hz, a maximum voltage and power level of 104 mV and 342 μW have been obtained, respectively. Furthermore, operation frequency of the 2nd prototype can be tuned by properly adjusting the rubber springs. By changing the stiffness of the rubber springs, desired resonance frequency can be realized for both of the diaphragm, realizing the frequency up-conversion.

The proposed generator structure has been designed in micro scale and fabrication steps and process flow has been given in detail. The fabrication process has been almost completed, however, due to some problems in the final step; the fabrication of the devices could not be finalized. However, the problem is pointed out and a possible modification in the fabrication process flow has been proposed in order to eliminate the problem.

The achievement of this thesis study can be listed as,

- The frequency up-conversion concept has been improved by introducing a monolithic diaphragm instead of consecutive cantilevers.
- The voltage output levels have been increased through a larger available area for number of coil turns.
- The power output levels have been increased by enhancing the thickness of the coil layers by micro fabrication techniques.

- The macro prototypes of the proposed generator have been implemented as proof of concept for realizing the frequency up-conversion with two diaphragm structures.

This thesis work covers all the objectives that are planned to be undertaken stated at the proposal of the study excluding the completion of the micro fabrication. Following this, there are also some points that can be improved as a future work. Some of these points can be listed as;

1. Fabrication process flow should be reviewed and the problematic steps should be re-designed.
2. A further improvement in the structure could be done. Implementing two coil diaphragms into the design to increase the voltage and power levels (Figure 5.1) expressed as third generation.
3. Implementing piezoelectric materials into the design to reach higher power levels.
4. Integration with rectifying electronics. However, generated voltage level is low. On the other hand, the number of coil turns can easily be increased.

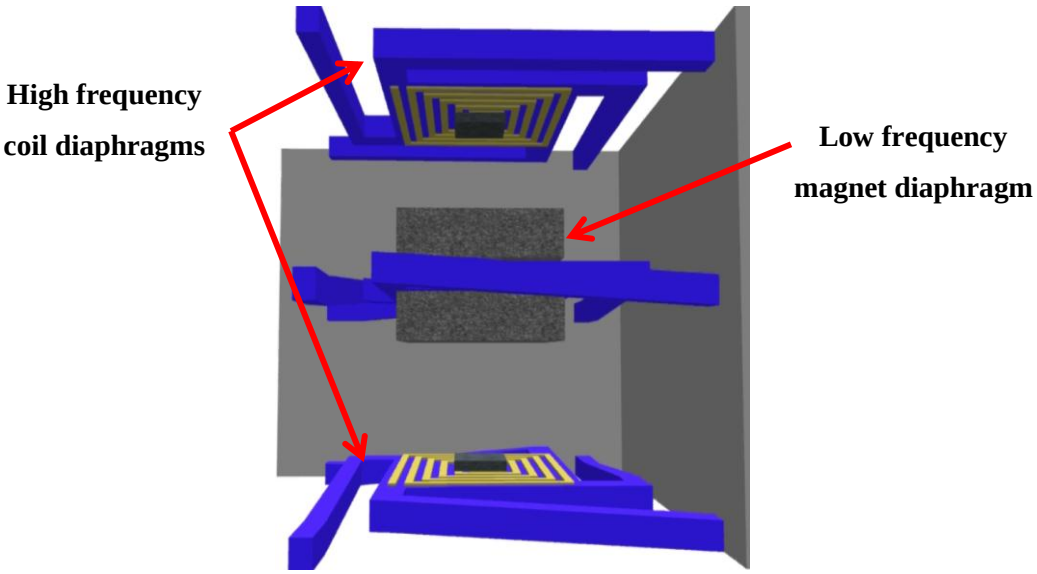

Figure 5.1. Third generation frequency up-conversion design.

REFERENCES

[1] J. A. Paradiso and T. Starner, "Energy Scavenging for Mobile and Wireless Electronics," *IEEE Pervasive Computing*, vol. 4, issue 1, pp. 18-27, Mar 2005.

[2] M. Mizuno and D. G. Chetwynd, "Investigation of a Resonance Microgenerator," *Journal of Micromechanics and Microengineering*, vol. 13, pp. 209–216, Mar 2003.

[3] N. N. H. Ching, H. Y.Wong, W. J. Li, P. H. W. Leong, and Z. Y.Wen, "A Laser-Micromachined Multi-Modal Resonating Power Transducer for Wireless Sensing Systems," *Sensors and Actuators A: Phys*ical, vol. 97–98, pp. 685–690, Nov 2001.

[4] A. Muhtaroğlu, A. Yokochi, and A. von Jouanne, "Integration of Thermoelectrics and Photovoltaics as Auxiliary Power Sources in Mobile Computing Applications," *Journal of Power Sources*, vol. 177, no. 1, pp. 239-246, Feb 2008.

[5] H. Külah and K. Najafi, "An Electromagnetic Micro Power Generator for Low-Frequency Environmental Vibrations," *17th IEEE International Conference on Microelectromechanical Systems (MEMS '04)*, pp. 237-240, Jan 2004.

[6] S. Roundy, "Energy Scavenging for Wireless Sensor Nodes with a Focus on Vibration to Electricity Conversion," *Ph.D., University of California, Berkeley*, 2003.

[7] IDTechEX, "Masterclass: Introduction to Energy Harvesting for Low Power Electronics," *Energy Harvesting and Storage Conference Europe 2011*, Jun 2011.

[8] S. Roundy, P. K. Wright, and J. Rabaye, "A Study of Low Level Vibrations as a Power Source for Wireless Sensor Nodes," *Computer Communications*, vol. 26, no. 11, pp. 1131–44, Jul 2003.

[9] T. Starner and J. Paradiso, "Human Generated Power for Mobile Electronics,"*Low Power Electronics Design*, pp. 1-35, 2004.

[10] T. Von Buren, P. Lukowicz, and Troster, "Kinetic Energy Powered Computing—An Experimental Feasibility Study," *Proceedings of 7th IEEE International Symposium on Wearable Computers ISWC '03*, pp. 22–24, Nov 2003.

[11] I. Sari, T. Balkan, and H. Külah, "A Micro Power Generator with Planar Coils on Parylene Cantilevers," *IEEE Ph.D. Research in Microelectronics and Electronics (PRIME) Conference*, Jun 2008.

[12] C.B. Williams and R.B. Yates, "Analysis of a Micro-Electric Generator for Microsystems," *Sensors and Actuators A: Physical*, vol. 52 issue 1-3, pp. 8–11, Mar 1996.

[13] C.B. Williams, R. C. Woods, and R. B. Yates, "Feasibility Study of a Vibration Powered Micro-Electric Generator," *IEE Colloquium on Compact Power Sources*, pp. 7/1 - 7/3, May 1996.

[14] M. El-Hami, P. Glynne-Jones, N. M. White, M. Hill, S. Beeby, E. James, A. D. Brown, and J. N. Ross, "Design and Fabrication of a New Vibration-Based Electromechanical Power Generator," *Sensors and Actuators A: Physical*, vol. 92, no. 1–3, pp. 335–342, Aug 2001.

[15] S. P. Beeby, R. N. Torah, M. J. Tudor, P. Glynne-Jones, T. O'Donnell, C. R. Saha, and S. Roy, "A Micro Electromagnetic Generator for Vibration Energy Harvesting," *Journal of Micromechanics and Microengineering*, vol. 17, no. 7, pp. 1257–1265, Jul 2007.

[16] I. Sari, T. Balkan, and H. Külah, "An Electromagnetic Micro Power Generator for Wideband Environmental Vibrations," *Sensors and Actuators A: Physical*, vol. 145-146, pp. 405-413, Aug 2008.

[17] R. Amirtharajah and A. P. Chandrakasan, "Self-Powered Signal Processing using Vibration-Based Power Generation," *IEEE Journal of Solid-State Circuits*, vol. 33, no. 5, pp. 687–695, May 1998.

[18] K. Nakano, T. Saito, A. Nakayama, and T. Kurose, "A Portable Generator using Vibration due to Human Walking," *Tech. Dig. 2002 Int. Workshop Power MEMS (Power MEMS 2002)*, pp. 114–117, Nov 2002.

[19] H. Külah and K. Najafi, "Energy Scavenging from Low-Frequency Vibrations by using Frequency Up-Conversion for Wireless Sensor Applications," *IEEE Sensors Journal*, vol. 8, no. 3, pp. 261–268, Mar 2008.

[20] I. Sari, T. Balkan, and H. Külah, "An Electromagnetic Micro Power Generator for Low Frequency Environmental Vibrations Based on the Frequency Up-Conversion Technique," *Journal of Microelectromechanical Systems*, vol. 19, no. 1, pp. 14–27, Jan 2010.

[21] I. Sari, "Design, Fabrication and Implementation of a Vibration Based MEMS Energy Scavenger for Wireless Microsystems," Ph.D., METU, Sep 2008.

[22] K. Najafi, T. Galchev, E. E. Aktakka, R. L. Peterson, and, J. McCullagh, "Microsystems for Energy Harvesting," *16th International Conference on Solid State Sensors, Actuators, and Microsystems (Transducers'11)*, pp. 1845-1850, Jun 2011.

APPENDIX A

FABRICATION PROCESS OUTLINE

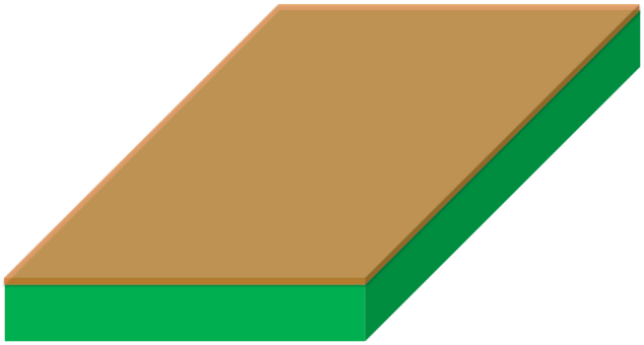

Parylene deposition

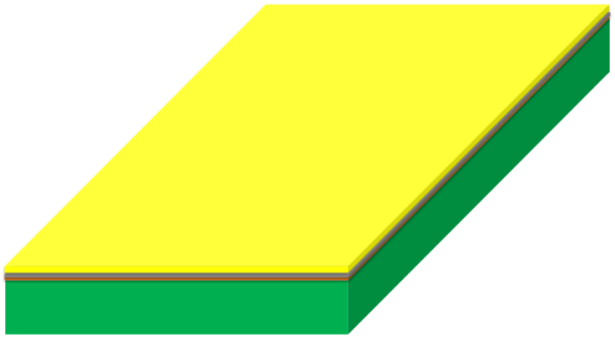

Au/Ti sputtering

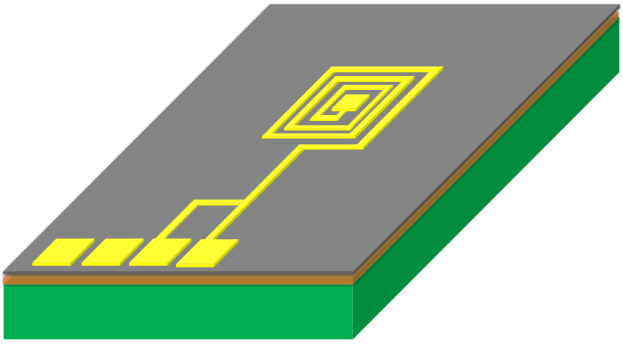

Patterning Au

Figure A.1. Fabrication process outline of the micro generator.

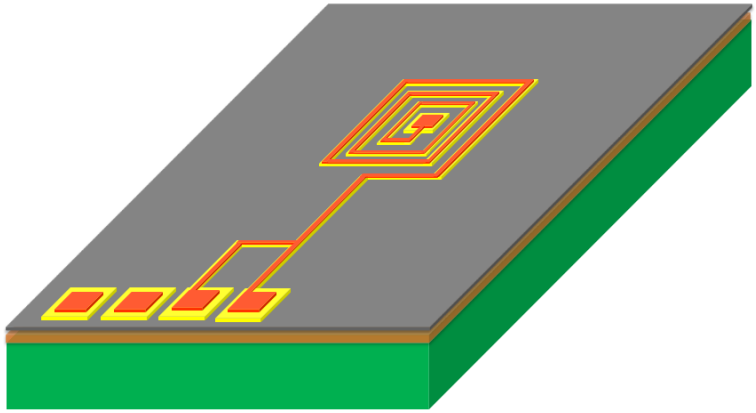

Copper Electroplating

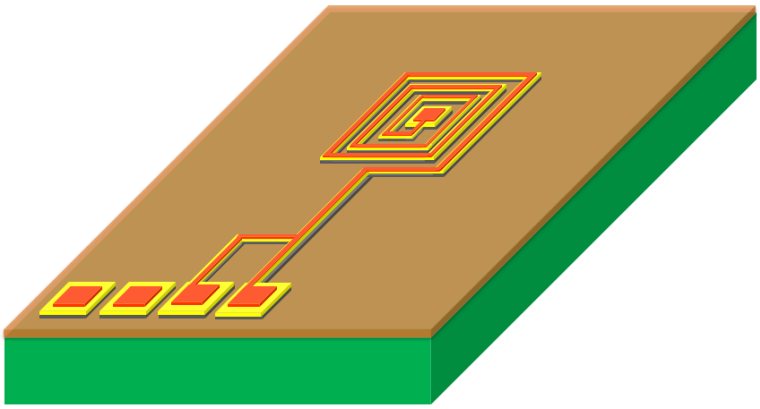

Ti etch

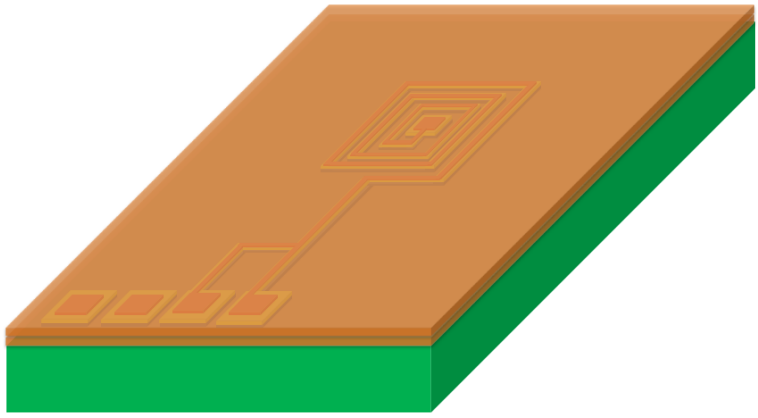

Parylene deposition

Figure A.1. (cont'd).

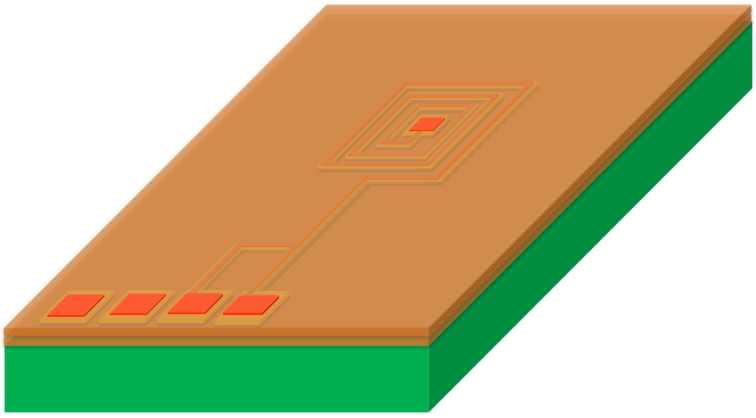

Via opening on parylene

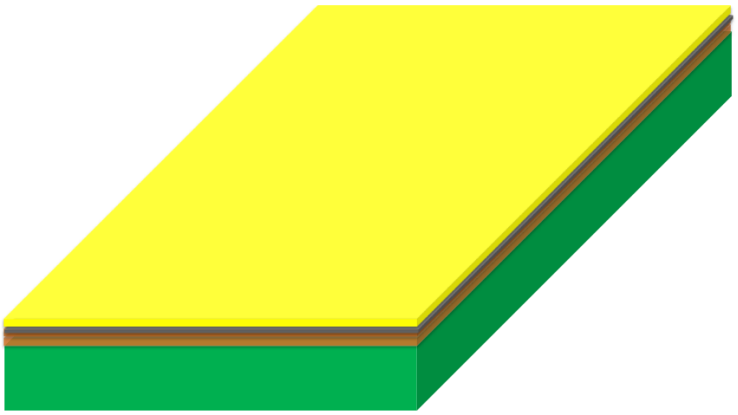

Au/Ti sputtering

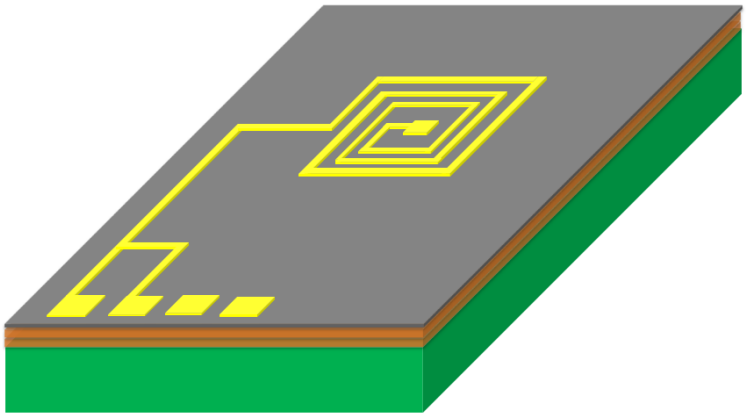

Patterning Au

Figure A.1. (cont'd).

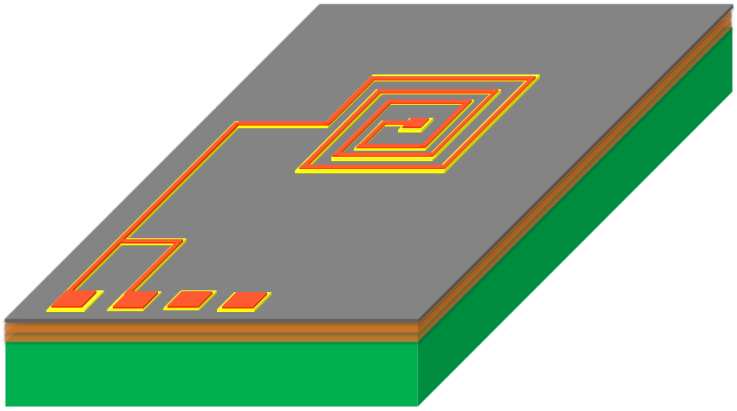

Copper electroplating

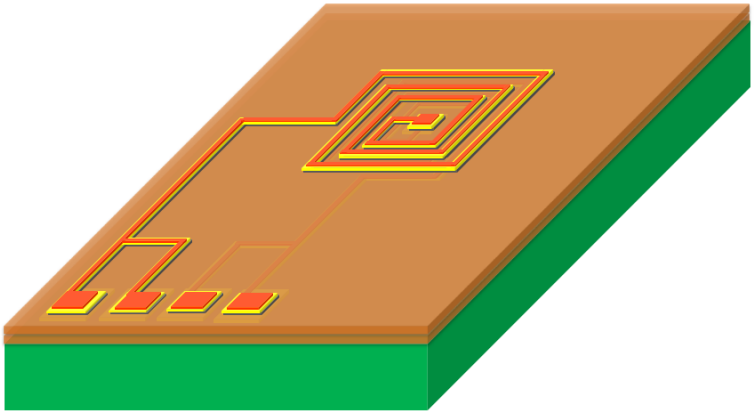

Ti etch

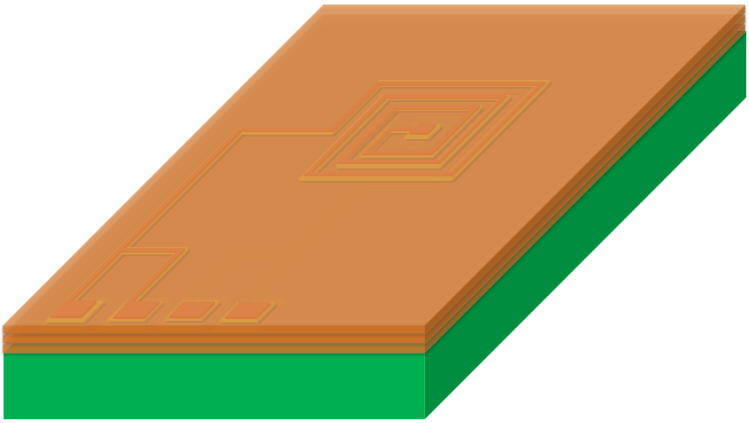

Parylene deposition

Figure A.1. (cont'd).

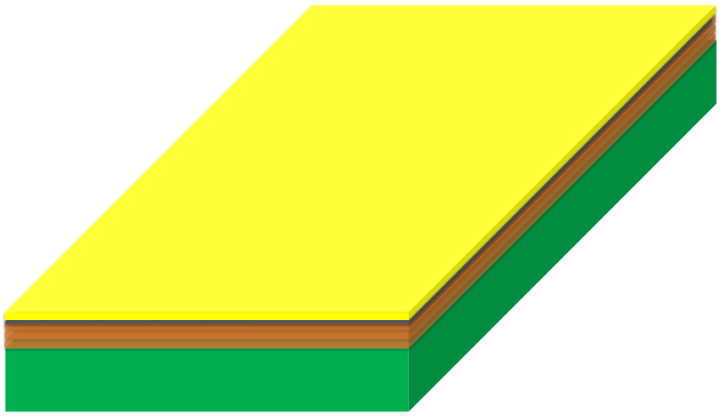

Au/Ti sputtering

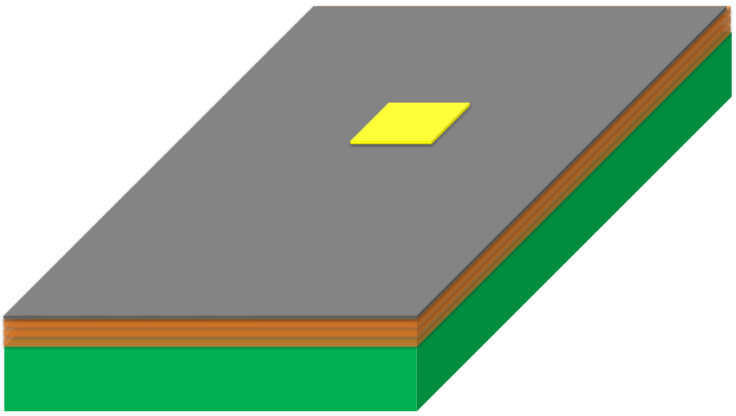

Patterning Au

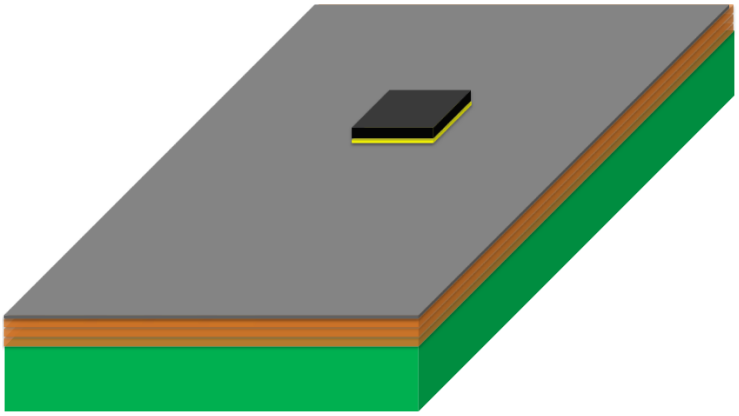

Nickel electroplating

Figure A.1. (cont'd).

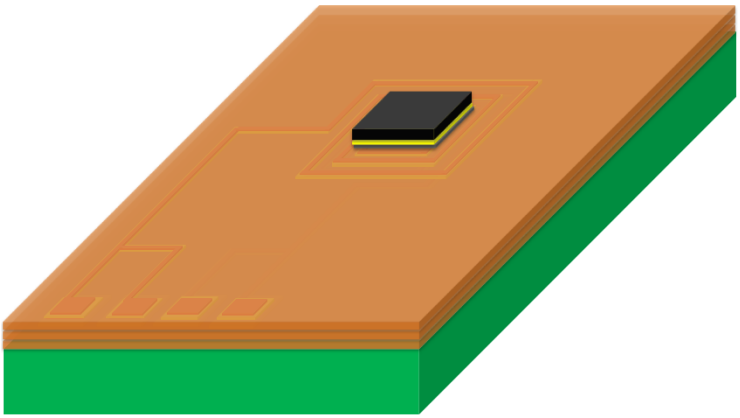

Ti etch

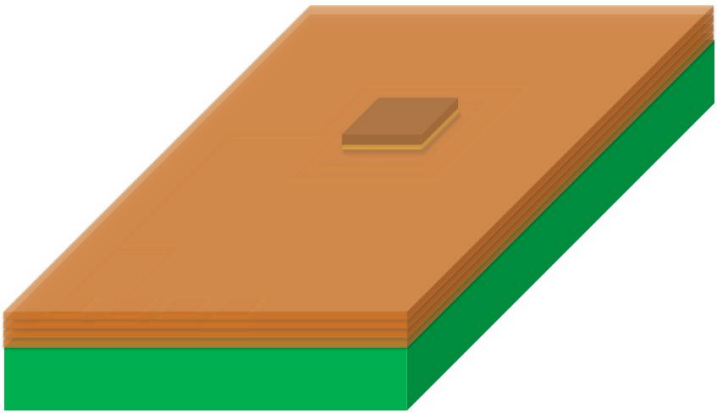

Parylene deposition

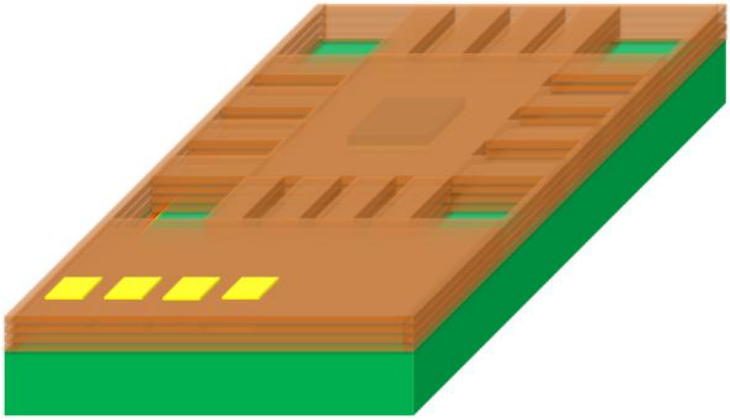

RIE to pattern parylene

Figure A.1. (cont'd).

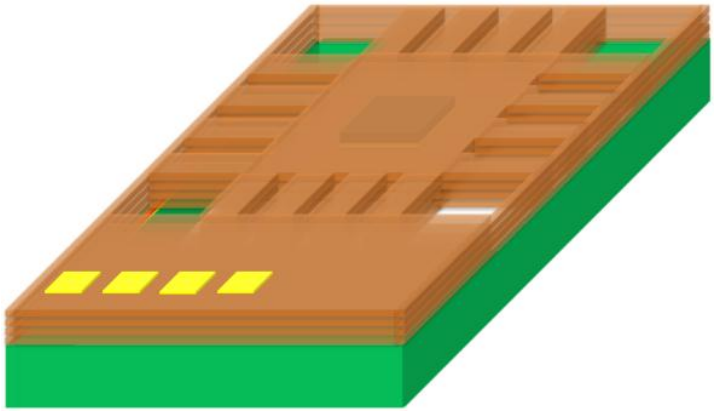

DRIE to release the device

Figure A.1. (cont'd).

APPENDIX B

FABRICATION PROCESS FLOW

Table B.1. Process steps for sputtering and patterning Au/Ti.

Ti-Au sputtering before copper electroplating	Parylene Deposition (5µm)	SP:15 PLA1:10, use A-174-Silane (Backside protection with dicing tape)
	Dehydration	Right before sputter, dehydrate 40mins. in oven @90^{o}C, cool down in desiccator for 10 mins.
	Ti Sputter (40nm)	Time1: 120 sec., Time2: 270 s., MFC1: 2.5 sccm, 300W
	Au Sputter (125 nm)	Time1: 120 sec., Time2: 130 s., MFC1: 6.2 sccm, 300W
	Lithography	
	Dehydration	Dehydrate 40 mins. in oven @90^{o}C, Cool down in desiccator for 10 mins.
	Primer Spin	Primer@2000 rpm, t=30s.
	PR Spin	S1813 @4000 rpm, t=30s.
	Softbake	Softbake t=60s over contact hotplate @T=115^{o}C
	Expose	Expose 7 sec. (Vacuum contact)
	Develop	MF319, 65 s.
	Hardbake	Hardbake (for Metal etch) @90^{o}C for 10 mins. Cool down in desiccator 5 mins.
	Au Wet Etch	Au etchant 30-40 s.
	PR Strip	SVC

Table B.2. Process steps for Cu electroplating.

Copper electroplating	Dehydration	Right before electroplating, dehydrate 10 mins. İn oven @90^{o}C, cool down in desiccator for 5 mins.
	Lithography	
	Primer Spin	Primer@2000 rpm, t=30s.
	PR Spin	AZ9260 @1700 rpm, t=60s. (12.5 μm aimed) + EBR with the same settings.
	Softbake	Softbake @90^{o}C for 30 mins. in oven
	Expose	Expose 35 sec. (Vacuum contact)
	Develop	AZ 826 MIF, 5 mins.
	PR thickness measurement	Veeco Dektak 8
	Cu Electroplating (10 μm)	T=18^{o}C, A=20.44 dm^{2}, duty=0.03, T_{on}=0.1 ms, T_{off}=2.4 ms, I_{avg}=44.2 mA
	Electroless gold deposition	T=85^{o}C, 20 mins.
	PR Strip	Acetone + IPA +DI Water.
	Ti Wet Etch	Ti etchant, prepare 100 ml (80% H_2O+10% HF+10% H_2O_2), 25 ml Ti etchant + 1575 ml DI H_2O, ~80 sec.

Table B.3. Process steps for opening vias on parylene.

Parylene vias	Parylene Deposition (5μm)	SP:15 PLA1:10, use A-174-Silane (Backside protection with dicing tape)
	Dehydration	Right before sputter, dehydrate 40mins. in oven @90^{o}C, cool down in desiccator for 10 mins.
	Lithography	
	Primer Spin	Primer@2000 rpm, t=30s.
	PR Spin	AZ9260 @1500 rpm, t=60s. (10 μm aimed) + EBR with the same settings.
	Softbake	Softbake @90^{o}C for 30 mins. in oven
	Expose	Expose 35 sec. (Vacuum contact)
	Develop	AZ 826 MIF, 6-7 min.
	Hardbake	No
	PR thickness measurement	Veeco Dektak 8
	Parylene Etch by RIE	15 min., O_2 Plasma, 100 sccm, 100 mTorr, 100 Watt
	PR Strip	Acetone + IPA + DI Water

Table B.4. Process steps for sputtering and patterning Au/Ti.

Ti-Au sputtering before copper electroplating	Parylene Deposition (5µm)	SP:15 PLA1:10, use A-174-Silane (Backside protection with dicing tape)
	Dehydration	Right before sputter, dehydrate 40 mins. in oven @90^{o}C, cool down in desiccator for 10 mins.
	Ti Sputter (40nm)	Time1: 120 sec., Time2: 270 sec., MFC1: 2.5 sccm, 300W
	Au Sputter (125 nm)	Time1: 120 sec., Time2: 130 sec., MFC1: 6.2 sccm, 300W
	Lithography	
	Dehydration	Dehydrate 40 mins. in oven @90^{o}C, Cool down in desiccator for 10 mins.
	Primer Spin	Primer@2000 rpm, t=30s.
	PR Spin	S1813 @4000 rpm, t=30s.
	Softbake	Softbake t=60s over contact hotplate @T=115^{o}C
	Expose	Expose 7 sec. (Vacuum contact)
	Develop	MF319, 65 sec.
	Hardbake	Hardbake (for Metal etch) @90^{o}C for 10 mins. Cool down in desiccator 5 mins.
	Au Wet Etch	Au etchant 30-40 sec.
	PR Strip	SVC

Table B.5. Process steps for second Cu electroplating.

Copper electroplating	Dehydration	Right before electroplating, dehydrate 10 mins. in oven @90^{o}C, cool down in desiccator for 5 mins.
	Lithography	
	Primer Spin	Primer@2000 rpm, t=30s.
	PR Spin	AZ9260 @1700 rpm, t=60s. (12.5 μm aimed) + EBR with the same settings.
	Softbake	Softbake @90^{o}C for 30 mins. in oven
	Expose	Expose 35 sec. (Vacuum contact)
	Develop	AZ 826 MIF, 5 min.
	Hardbake	No
	PR thickness measurement	Veeco Dektak 8
	Cu Electroplating (10 μm)	T=18^{o}C, A=19.27 dm^{2}, duty=0.03, T_{on}=0.1 ms, T_{off}=2.4 ms, I_{avg}=46.8 mA
	Electroless gold deposition	T=85^{o}C, 20 mins.
	PR Strip	Acetone + IPA +DI Water.
	Ti Wet Etch	Ti etchant, prepare 100 ml (80% H_2O+10% HF+10% H_2O_2), 25 ml Ti etchant + 1575 ml DI H_2O, ~80 sec.

Table B.6. Process steps for Ni electroplating.

Ni electroplating	Dehydration	Right before electroplating, dehydrate 10 mins. in oven @90^{o}C, cool down in desiccator for 5 mins.
	Ti Sputter (40nm)	Time1: 120 sec., Time2: 270 sec., MFC1: 2.5 sccm, 300W
	Au Sputter (125 nm)	Time1: 120 sec., Time2: 130 sec., MFC1: 6.2 sccm, 300W
	Lithography	
	Dehydration	Dehydrate 40 mins. in oven @90^{o}C, Cool down in desiccator for 10 mins.
	Primer Spin	Primer@2000 rpm, t=30s.
	PR Spin	AZ9260 @1500 rpm, t=60s. (11 μm aimed) + EBR with the same settings.
	Softbake	Softbake @90^{o}C for 30 mins. in oven
	Expose	Expose 40 sec. (Vacuum contact)
	Develop	AZ 826 MIF, 6 min.
	O_2 plasma	O_2 Plasma @ 0.2-0.3 Torr for 1-2 mins.
	Ni Electroplating (9 μm)	T=50^{o}C, A=15.04 dm^2, duty=0.03, T_{on}=0.1 ms, T_{off}=2.4 ms, I_{avg}=60 mA
	Au Wet Etch	Au etchant 25-32 s.
	Ti Wet Etch	Ti etchant, prepare 100 ml (80% H_2O+10% HF+10% H_2O_2), 25 ml Ti etchant + 1575 ml DI H_2O, ~80 sec.
	PR Strip	Try Acetone + IPA, else use SVC

Table B.7. Process steps for patterning parylene by RIE.

Parylene pattern	Parylene Deposition (5μm)	SP:15 PLA1:10, use A-174-Silane (Backside protection with dicing tape)
	Dehydration	Right before sputter, dehydrate 40mins. In oven @90^{o}C, cool down in desiccator for 10 mins.
	Primer Spin	Primer@2000 rpm, t=30s.
	PR Spin	AZ9260 @1500 rpm, t=60s. (11 μm aimed) + EBR with the same settings.
	Softbake	Softbake @90^{o}C for 30 mins. in oven
	Expose	Expose 40 sec. (Vacuum contact)
	Develop	AZ 826 MIF, 6 min.
	O_2 plasma	O_2 Plasma @ 0.2-0.3 Torr for 1-2 mins.
	Hardbake	No
	Parylene Etch by RIE	30 + 30 mins., O_2 Plasma, 100 sccm, 100 mTorr, 100 Watt
	PR Strip	Acetone + IPA + DI Water

Table B.8. Process steps for the release of the devices by DRIE.

Backside etch	Backside Lithography	
	Dehydration	Right before sputter, dehydrate 40mins. in oven @90^{o}C, cool down in desiccator for 10 mins.
	Primer Spin	Primer@2000 rpm, t=30s.
	PR Spin	AZ9260 @900 rpm, t=30s. (20 μm aimed)
	Softbake	Softbake @90^{o}C for 20 mins. in oven
	Expose	Expose 65 sec. (Vacuum contact)
	Develop	AZ 826 MIF, 6 min.
	Reconstruct EB at the backside	Reconstruct edge bead at the back with AZ9260 @750 rpm (spin PR to the edge only), wait 5 mins., softbake @100^{o}C, t=5 mins., cool down in desiccator
	Attachment of handle wafer	Attach handle wafer to the process wafer by thermal gress over hot plate @115^{o}C
	Backside SiO_2 etch by RIE	Use the DRIE mask, 100 mTorr, 300 W, Chiller Temp.=20^{o}C, CF_4=12 sccm, CHF_3=38 sccm, t=~6 mins.
	Backside Si etch by DRIE	About 100 mins.
	Release	Keep the wafer in acetone about one day